NACA

RESEARCH MEMORANDUM

EFFECT OF SURFACE ROUGHNESS ON CHARACTERISTICS OF SPHERICAL SHOCK WAVES

By Paul W. Huber and Donald R. McFarland

Langley Aeronautical Laboratory
Langley Field, Va.

CLASSIFIED DOCUMENT

NATIONAL ADVISORY COMMITTEE
FOR AERONAUTICS

WASHINGTON
May 25, 1955

NATIONAL ADVISORY COMMITTEE FOR AERONAUTICS

RESEARCH MEMORANDUM

EFFECT OF SURFACE ROUGHNESS ON CHARACTERISTICS OF SPHERICAL SHOCK WAVES

By Paul W. Huber and Donald R. McFarland

SUMMARY

An investigation has been conducted on a small-scale test layout in which direct observation of the shock-wave movement with time could be made in order to determine the effects of surface roughness on the characteristics of spherical shock waves. Data were obtained with 15-gram pentolite charges at four heights of burst, both for a smooth surface and for a surface completely covered with pyramid-shaped roughness elements. The observations resulted in determinations of shock peak overpressure and Mach stem height as a function of distance for each test condition.

Comparison of the smooth-surface data with those obtained for the extremely rough condition showed a small net effect of roughness on the shock peak overpressures at the surface for all burst heights, the effect being to lower the overpressures. The effect of surface roughness on the Mach stem formation and growth was to delay the formation at the greatest charge height and to lower the height of the Mach stem for all heights of burst.

Comparison of the free-air shock peak overpressures with larger scale data showed good similarity of the overpressure-distance relationships. The data did not fit a geometrical similarity parameter for the path of the triple point at different heights of burst suggested by other investigators. A simple similarity parameter (relating the horizontal distance to the theoretical point of Mach formation) was found which showed only a small influence of burst height on the path of the triple point.

While the data presented provide knowledge of the effect of many surface-roughness elements on the overall shock characteristics, the data do not provide insight into the details of the air-flow characteristics along the surface, nor the relative contribution of individual roughness elements to the results obtained.

INTRODUCTION

In studying the motion and properties of a shock wave moving past a body or along a surface, it is usually expedient to regard the surface as rigid and the flow as nonheat-conducting and nonviscous. Under this assumption, the problem can be limited to one of reflection and diffraction of the wave by depending upon the shape of the surface and its relationship to the oncoming wave and one in which the fluid flow over the surface behind the wave is free of wake or boundary layer. In reality, however, some energy exchange occurs between the fluid and the surface due to heat transfer, cavitation, and so forth, and some increase in the fluid entropy takes place near the surface because of viscous action. The latter effect is present to some degree, regardless of the rigidness or heat-insulating properties of the surface, and the extent of this action is then dependent upon the fluid properties and surface roughness. To attempt to calculate these viscous effects in a three-dimensional unsteady flow such as this would be beyond the scope of application of any existing theories.

In reference 1, measurements of Mach stem heights over smooth hard-packed dirt and smooth dry sand indicated that the path of the triple point in the case of dry sand was lower than that for hard-packed dirt. While no explanation for this difference was advanced, it was speculated that, due to its porosity, the sand may act as an absorber rather than as a rigid reflector. Some differences in the test conditions were also noted. Higher ambient air temperatures were indicated for the dry-sand tests, which could indicate slightly weaker shock strengths. Possibly, in the case of dry sand some erosion of the sand also took place in the air flow behind the shock. In reference 2, measurements of Mach stem heights over rows of solid walls located on a smooth surface indicated that the formation of the Mach stem was delayed and the path of the triple point was lowered by the walls. Here the differences might be resolved into two, or a combination of two, categories. One factor could be a pure-wave-diffraction problem in which temporary lowering of the stem occurs due to the reflections about the walls, but far from the walls little, if any, effect on the shock would be noted since upstream and downstream wave reflections would essentially cancel each other. The other factor could be viscous air-flow losses as a result of separation and vortices from the air flow over the walls, which by some wave-viscous interaction could weaken the strength of the shock.

The effect of patterned surface roughness on the overpressure characteristics of plane shock waves was experimentally determined in a shock tube in a study made at the Langley Aeronautical Laboratory by Paul W. Huber, Donald R. McFarland, and Philip Levine. Attenuation of the

shock-wave overpressure of as much as 30 percent was measured for a roughness size of $\frac{1}{4}$ inch. In this case of channel-type flow, however, any wave quantities generated near the surface as a result of viscous action must remain confined within the walls of the shock tube, and any such net effect must propagate along the axis of the shock tube. If the shock-tube flow is many times longer than the cross-sectional dimension, as is usually the case, the shock strength at all points across the channel is almost equally affected by all previous viscous surface action along the flow path. Reasonably, then, the magnitude of the attenuation in this quasi-one-dimensional type of flow can be expressed in terms of the surface-volume ratio of the shock tube (reciprocal of hydraulic radius in pipe flow).

In the case of a spherical shock wave moving over a surface, however, three dimensionality of the pressure and flow patterns exists in the neighborhood of the surface so that concepts of wave attenuation established by the shock-tube tests are not applicable. For this reason, an investigation of the effects of surface roughness on spherical shock waves was made in the Gas Dynamics Branch of the Langley Laboratory by duplicating, as reasonably as practicable on a small scale, the actual shock-wave conditions.

The scale of this investigation was chosen so as to allow the safe use of instrumentation and equipment under controlled laboratory conditions. It was felt that, even if the selection of such a small scale resulted in some variance of the data with large-scale blast data, the comparison of rough- and smooth-surface data could still be made. In this investigation roughness-element heights of $\frac{1}{4}$ inch would be equivalent to about 23.5 feet for a charge of 20 kilotons of trinitrotoluol (TNT). In order to obtain the maximum effect of roughness and for simplicity in evaluation of the experimental results, complete coverage of the surface with roughness elements was chosen as the rough surface condition to be used.

SYMBOLS

a	velocity of sound, ft/sec
p	pressure, lb/sq in. abs
S	shock propagation velocity, ft/sec
γ	ratio of specific heat at constant pressure to specific heat at constant volume

d horizontal distance from charge, in. or ft

h height above surface, in. or ft

α angle between horizontal and tangent to incident wave at triple point, $\tan^{-1}\frac{d_y}{h_c - h_y}$, deg

ϕ angle between horizontal and line connecting d_o and Mach intersection, $\tan^{-1}\frac{h_y}{d_y - d_o}$, deg

Subscripts:

1 ahead of shock

2 immediately behind shock

c charge

y point of intersection of incident, reflected, and Mach shocks

e at theoretical limit of regular reflection; for example, $\alpha_e = \tan^{-1}\frac{d_o}{h_c}$

o at theoretical limit of regular reflection; for example, d_o

EXPERIMENTAL METHOD

At any instant of time, the velocity of propagation of a point on any wave can be expressed in terms of the fluid properties existing locally about that point. In the case of a shock wave, the velocity of propagation with respect to the fluid ahead, along an axis normal to the wave, is expressed in terms of the pressure ratio across the wave, the velocity of sound, and the specific-heat ratio of the fluid as

$$S = a_1\left[\frac{\gamma - 1}{2\gamma}\left(\frac{\gamma + 1}{\gamma - 1}\frac{p_2}{p_1} + 1\right)\right]^{1/2} \tag{1}$$

where γ of the fluid is assumed invariant with temperature.

In the case of a shock wave moving into a fluid which is stationary, equation (1) also represents the velocity of propagation of the shock with respect to an observer.

If the velocity of propagation, undisturbed pressure, specific-heat ratio, and sound velocity are known, the shock peak overpressure can be expressed from equation (1) as

$$p_2 - p_1 = p_1\left\{\frac{2\gamma}{\gamma + 1}\left[\left(\frac{S}{a_1}\right)^2 - 1\right]\right\} \tag{2}$$

Inasmuch as the undisturbed properties of the fluid are known and can be held constant during a controlled laboratory blast, the variation of shock peak overpressure with time readily results from measurements of the variation of shock-wave-propagation velocity with time. This variation was obtained by graphically determining slopes from plots of shock-wave position with time. These data points were obtained directly from schlieren photographs of the wave taken at eight regular and accurately known time intervals for each blast. This equipment is referred to hereinafter as the NACA nine-channel spark and was developed at the Langley Laboratory by Joseph Burlock.

With schlieren photographs from the NACA nine-channel spark, the free-air shock peak overpressure, Mach shock peak overpressure along the surface, and Mach stem height could be obtained as a function of time and position. The regular reflected peak overpressures could not be obtained by using this method since the velocity of the reflection point along the surface, for the case of regular reflection, is not related to the reflected peak overpressure.

Pressure-time measurements at seven surface locations were also made for each blast at the highest charge location by using rapid-response flush-mounted gages. These data served as check points for the shock overpressures obtained by the velocity method and, in addition, provided measurements of the variation of pressure with time behind the shock wave so that the duration of positive overpressure could be determined.

APPARATUS AND PROCEDURE

A schematic diagram of the apparatus and instrumentation is shown in figure 1, and photographs of the apparatus are shown in figure 2.

The wave table shown in figures 1 and 2 is the area over which the charges were detonated and the wave characteristics experimentally

determined. This table was fabricated from 2-inch boiler plate machined smooth and flat on the upper surface. The table was 12 feet square and was supported by 4 large I-beams inbedded in concrete, so that the under surface of the table was accessible for mounting the pressure instrumentation and running electrical leads.

Roughness blocks were cast of 1-foot-square aluminum $\frac{1}{2}$ inch thick placed with the block edges parallel to the table edges to cover the upper surface of the table. The rough surface consisted of continuous rows of pyramid-shaped elements of $\frac{1}{4}$-inch height and $\frac{1}{2}$- by $\frac{1}{2}$-inch base which were arranged to cover completely the surface of the block. These rows were orientated at an angle of 45° to the block edges and to the blast line. (See fig. 1.)

Directly over the center of the table and at any predetermined height, a $13\frac{1}{2}$-gram sperical-cast bare 50/50 pentolite charge was detonated. This charge has a detonator well which was 5/16 inch in diameter and 6/10 inch deep. The charges were suspended from a support arm by placing the charge in a mesh net and then hanging the net to a hooked metal rod which could be raised and lowered in the support arm. (See fig. 2(b).) The support arm was located in a plane at the center of the table and perpendicular to the blast line and consisted of a crescent-shaped plate of $\frac{1}{2}$-inch steel, one end of which was bolted to the tabletop at a point 3 feet away from the blast line and the other end of which was $3\frac{1}{2}$ feet above the table. These distances were sufficient to prevent any reflected waves from the support arm from overtaking the shock as seen along the blast line during the time of observation. The pentolite charge was detonated by an instantaneous electric blasting cap having a shaped charge. This cap was inserted 6/10 inch into the detonator well of the pentolite charge. The axis of the cap was perpendicular to the blast line and parallel to the tabletop, and lead wires were run up and along the top of the support arm. This cap was estimated to contain a charge of explosive energy equivalent to about 1.5 grams of pentolite.

A row of seven pressure pickups was located along the blast line as shown in figures 1 and 3. These pickups were flush-mounted capacitor-type frequency-modulated carriers (Rutishauser Pressure Pickup, Type HR-3, in conjunction with the Rutishauser Electronic Pickup Indicator, Type ST-127A) and used diaphragms with natural frequencies of 10,000 to 30,000 cps. When roughness was used, the pickups were inserted in the roughness to one-third the pyramid height, and the tap drill for the pickup was drilled through the roughness block. (See fig. 3.) The seven-gage

outputs were simultaneously recorded on two synchronous motor-drum cameras which photographed 2 four-channel oscilloscopes. These pickups could be statically calibrated by mounting them in a calibration box and recording the oscilloscope traces for a series of static pressures. Calibration up to 15 pounds per square inch absolute could be made with the pickups in position on the table by evacuating the inside of the gage. These pickups measure pressure within an accuracy of about 2 percent of the full-scale pressure range for each diaphragm used.

Eight schlieren optical systems were arranged, as shown in figures 1 and 3, so that movement of the shock wave along the blast line could be recorded photographically. Two complete optical systems were common to each pair of parabolic mirrors, and the mirror sets were placed along the blast line at increasing distances and alternately on opposite sides of the charge. In this manner, nearly complete coverage of an area of 12 inches above the blast line extending from a point 6 inches from the center of the table to the edge of the table could be obtained optically.

The first three sets of mirrors had 16-inch diameters and 90-inch focal lengths, and the fourth set had an 18-inch diameter and a 105-inch focal length. Both the sources and knife edges were offset 3/8 inch from the optical center of the system which produced an angularity of the light beam of less than $1/4^{\circ}$. One 5- by 7-inch camera focused on the blast line and was used to record the images of each pair of optical systems.

The eight high-voltage sparks used for light sources of the schlieren system were electronically controlled to fire at any predetermined firing rate by means of the NACA nine-channel spark. This timer consisted of an electronic ring counter controlled by a signal generator so that the ring counter would produce a spiked pulse at a precise point of each signal cycle in successive channels of the timer. Each pulse would then fire a high-voltage thyratron tube located in one of the eight high-voltage power supplies to the sparks. The ionization time of the spark sources was held at a minimum by means of radioactive paint on the electrodes. The response of the NACA nine-channel spark and spark source to a given signal input is believed to be consistent within a few microseconds.

The first of the nine pulses was used to initiate an interval-delay timer which controlled the firing circuit for the detonator so that the remaining eight pulses would be synchronized to the shock movement along the table. This initial pulse also controlled the electronic shutter of the oscilloscopes so that the pressure-gage traces would be recorded for a period of one revolution of the drum cameras. Also recorded on the drum cameras in the earlier tests was the trace from a photomultiplier tube which was mounted to face the fireball. Two 5- by 7-inch still

cameras were placed so as to record a time-integrated photograph of the fireball from two views 90° apart.

In order to obtain accurate measurements of shock position from the schlieren photographs and for convenience in adjustment of the optics and identification of the film, four small steel pins and two tightly stretched piano wires were located along each of the two edges of the table parallel to the blast line as shown in figures 1 and 3. These pins and wires appear in the schlieren photographs and provide a reference point and length scale for each record. Because of the slight angularity of the schlieren light beams, the pair of steel pins common to each system would not appear superimposed on the film so that, in order to obtain a reference point on the blast line, it is necessary to take a point halfway between the images of the pins. The tops of the pins were bent so that the schlieren photograph showing the pins bent away from each other was the earlier of the two pictures in each set. A frequency counter was used to read the frequency of the signal generator and could be stopped immediately after a detonation. The stability of the signal generator and accuracy of the counter was such that the frequency was known to about one part in 1,200.

Insofar as was possible, the electronic equipment and instrumentation was located in a control house constructed about 15 feet away from the wave table. It was necessary, however, for the optical systems and high-voltage equipment to be located near the table, and in these cases plywood shielding was used to protect against copper fragments from the detonator caps and to provide for light shielding from the fireball. The cameras were also shielded against reflected light from the room, and solenoid-operated camera shutters were located directly behind the knife edges.

Preliminary to each series of detonations, the charge to be used was weighed to the nearest 0.01 gram with a chemical balance. Then the pressure gages were calibrated statically by both of the methods mentioned previously at a series of pressures which would cover the pressure range of each gage. Immediately before the detonation one calibration pressure trace for each gage using the evacuation method was superimposed on the drum-camera record.

The pentolite charge was suspended over the center of the table by means of a plumb line, and the height of charge was measured with a scale to the nearest 1/32 inch. (See fig. 2(b).) When roughness was used, the height of charge was measured from a point at one-third the pyramid height, the justification being that this would be the location of a smooth surface of equal displacement.

Immediately prior to a detonation the signal generator was set to the desired frequency and the delay of the firing circuit set to the

desired value. The temperature and pressure in the laboratory were recorded and all fans and ventilators shut off. The drum cameras were started, the room lights were shut off, and the shutters of the schlieren and still cameras were opened. Immediately after the detonation the signal-generator frequency was recorded.

Data were read from the drum-camera and schlieren films by means of a comparator. The accuracy of measurement of the films was better than 0.01 inch with this method. The peak-overpressure readings from the drum-camera records were obtained by fairing through the mean values of the gage-ringing oscillations. (See figs. 4(a) and 4(b).)

RESULTS AND DISCUSSION

A typical set of schlieren photographs showing the shock-wave movement along the smooth surface for a charge height of 2 feet is shown in figure 4(c) and along the rough surface in figure 4(d). The photographs taken on the left side of the table are shown in reversed direction so as to show all the waves moving from left to right. Typical pressure records are shown in figures 4(a) and 4(b) for both a smooth surface and rough surface detonation, respectively, for a charge height of 2 feet.

A typical time-distance history of the shock movement along the surface of the table and in free air taken from figure 4(c) is plotted in figure 5. The surface distance was measured horizontally from the center of the table to the point of intersection of the blast with the surface. The free-air distance was measured radially from the center of the charge to any convenient point on the incident shock wave, but not directly at the triple point. In both cases, the measurements were made at the extreme forward edge of the shock front. Selection of a more rearward point on the shock front would be doubtful because of possible diffraction effects of the light passing through the wave. The values of time which are plotted are taken from the frequency-counter readings and start from the time the first pulse of the NACA nine-channel spark is fired. As is the case in figure 4(c) and 4(d), the wave was seldom in the field of view in the first schlieren photograph, so that only seven experimental points could be plotted for each curve. The time at zero free-air distance, which corresponds to firing the charge, is obtained from the photocell record and includes the interval-delay timer and the delay of the detonator. This point is plotted to aid in the fairing of the free-air curve. The delay of the detonator was kept quite constant in these tests (about 50 microseconds) by using a high-voltage-discharge firing circuit. The time point shown for zero surface distance was estimated and plotted to aid in fairing the surface-distance curve. This point was obtained by finding the free-air shock-wave

velocity corresponding to the average of the distance from the charge to the table center and the distance from the charge to the first shock position, from accepted free-air data (ref. 3), and then substracting the resulting calculated travel time between these points from the first data point.

Slopes of the faired curves were then graphically obtained at each experimental data point on the plots, and the free-air shock peak overpressures obtained by this method using equation (2) are plotted in figure 6 for some typical tests. The pressures are corrected to standard atmospheric, and the distances are corrected to atmospheric pressure and reduced to 1 pound of pentolite, according to the usual scaling laws for blast data, by using the combined weight of cap and charge.

Figure 6 shows that, while there is some scatter of the data, in general the results agree very well with larger scale data such as reference 3. This fact would indicate that reducing the scale of the detonation to a much lower value than that used in previous shock-wave studies did not adversely affect the similarity of the blast pattern, which might be a little surprising in view of the larger ratio of cap size to charge size required for this work. Preliminary tests made with an electric cap small enough to be inserted completely into the charge showed a very poor reproducibility of the pressures so that the larger cap was actually necessary for consistent results. The time-integrated images of the fireballs obtained with the still cameras qualitatively verified this fact by showing a more nearly reproducible light pattern with the larger cap.

Mach shock peak overpressures along the surface were measured by this method for heights of burst of 2 feet, 1 foot, 6 inches, and 0.5 inch (reduced heights of 6.25, 3.125, 1.56, and 0.13 $ft/lb^{1/3}$) for both the smooth- and rough-surface conditions and are plotted in figures 7 to 10, respectively, reduced to standard atmospheric pressure and 1 pound of pentolite charge.

It can be seen from the fairing of the data-cluster arithmetic averages in figures 7 to 10 that, at all the heights of burst shown, a slightly lower Mach shock peak overpressure is obtained for the rough-surface condition. The magnitude of this difference, however, is less than the scatter of the individual data points and would not be easily distinguishable before averaging the data.

A plot of the peak overpressure along the surface as measured from the pressure-gage records, is shown in figure 11 for a reduced height of burst of 6.25 $ft/lb^{1/3}$ for both the smooth and rough surfaces. The faired curves taken from figure 7 are shown to aid in comparison of the pressure-pickup results with the NACA nine-channel-spark data. The

comparison is not particularly good, and the inconsistency in the pressure pickup data is felt to be due mainly to uncertainty in interpreting the pressure record. A considerable amount of high-frequency oscillation of the pressure trace (gage-diaphragm "ringing" excited by the shock) was present and, at the higher values of shock overpressure, was of a magnitude equal to or greater than the shock peak overpressure. Since damping of this oscillation required about $\frac{1}{2}$ millisecond, or 50 percent of the positive-overpressure time duration, and since the trace became very light at this high "writing" speed, the film reading was uncertain in this region. Basically, of course, this inability to obtain accurate pressure-pickup data must be attributed to the small scale of the experiment inasmuch as the same damping time in relation to longer positive-overpressure time durations would be less troublesome. Because of this difficulty and because it was felt that the NACA nine-channel-spark data are inherently more precise than pressure-pickup data, development of the pressure-pickup system was not pursued further. The time duration of the positive overpressure was obtained from each pressure record, and the averages of these measurements are plotted in figure 12 for the 6.25 $ft/lb^{1/3}$ reduced height of burst. (Smooth-surface pressure data were not available for the three smallest distances.) Only slight differences in time duration of the positive overpressure between the smooth- and rough-surface data are shown in figure 12.

By using the data from the NACA nine-channel-spark peak-overpressure measurements, the height-of-burst curves are plotted in figure 13 for both smooth- and rough-surface conditions and reduced to standard atmospheric pressure and 1 pound of pentolite charge. The data points shown are values taken from the faired curves in figures 7 to 10, and the solid and dashed curves in figure 13 are arbitrary fairings of these points for the smooth and rough surfaces, respectively. In figure 14 is shown a comparison of the height-of-burst curves of figure 13 with data points taken from reference 4. As was the case in figures 7 to 10, the differences in the smooth- and rough-surface data lie within the scatter of the individual data points taken from reference 4.

Measurements of the Mach stem heights were taken directly from the schlieren photographs and are plotted for both the smooth- and rough-surface conditions and for reduced heights of burst of 6.25, 3.125, and 1.56 $ft/lb^{1/3}$ in figures 15, 16, and 17, respectively. The arrows in these figures show the theoretical points of Mach stem formation. The curves drawn represent fairing of the arithmetic averages of the data-point clusters for each surface condition. It can be seen from these figures that the Mach stem height is lower for the rough-surface condition at all three heights of burst shown, and that the magnitude of the difference is in general greater than the scatter of the individual data points. These figures also show that the point at which the Mach stem

begins to rise is delayed in the case of roughness at the greatest charge height and possibly at all three heights of burst. To present these data in a form which is more readily extrapolated, the faired curves and data-point averages of figures 15 to 17 are shown in logarithmic coordinates in figure 18. It appears from this figure that, not only is the point of Mach stem formation possibly delayed for the rough condition at all heights of burst, but the point of rise for the case of the smooth surface and 6.25 $ft/lb^{1/3}$ reduced height of burst might also be delayed with respect to the theoretical rise point.

The faired data of figures 15 to 17 are compared with Mach stem measurements from references 1, 2, 5, 6, and 7 in figure 19. Figure 19 shows that the difference in Mach stem-height measurements for the smooth- and rough-surface conditions reported herein is less than the scatter of the reference data. Since the reference data were taken over surfaces not greatly different (with the exception of ref. 2) in comparison with the difference of surface conditions reported herein, it would not seem that the scatter of the reference data was due solely to surface conditions. There is a distinct difference, however, in the method used to obtain Mach stem height in this investigation with that used in the references. While the measurements obtained herein are the result of direct observation of the shock intersections, the method used previously involved extrapolation of gage-height against time-interval data to zero-time interval in order to obtain Mach stem height. This method frequently involved extrapolation of two or three point-data curves.

The effects of roughness on the surface-peak overpressure and Mach stem characteristics which have been determined in this investigation are the net effects of many roughness elements which contribute to the shock-propagation pattern. These results do not indicate what the relative contribution might be of any one, or one group, of roughness elements. Because of the small scale of this experiment, it would not be possible to resolve from the pressure traces or schlieren photographs the effects of earlier or later events on the overall pattern. It would seem logical to assume that individual elements or groups of elements do not have a strong effect on the overall shock characteristics in view of the small effect found for many elements. Because of the small scale of the tests and arrangement of the elements, it is also impossible to detect short-duration irregularities in shock movement (i.e., diffraction effects), such as probably occur locally each time a roughness element is encountered. What the effects of such things as roughness shape, or roughness spacing, might be on the shock-wave strength in the immediate vicinity of the elements cannot, therefore, be concluded.

Probably the most important result of surface roughness on shock-wave characteristics would be the retardation of air flow near the

surface (that is, within a region consisting of a few roughness heights above the surface). This so-called boundary layer in the air flow following the shock as a result of viscous air forces in the region of the roughness must result in some momentum loss to the system; however, since the amount of air flow involved in this region is small compared with the total air flow involved in the whole system, the net effect of this momentum loss on the shock-wave strength might be small. The amount of retardation of the air flow within this surface region, however, might very well be significant with regard to the drag forces and dynamic characteristics of bodies located in this region. Unfortunately, the determination of shock-wave strength does not yield much information as to these local air-flow velocities. To measure the air-flow velocities with any degree of certainty in small-scale blast investigations, such as these, would require instrumentation with smaller response times than any known to be available for velocity measurements.

The measurements of Mach stem height which have been presented herein are believed to represent more precise values than previous methods because these values are obtained from direct observation of the event. While such small-scale data might be intuitively looked upon with reservations, the free-air shock measurements have shown (see fig. 6) that scaling did not noticeably affect these wave-propagation data. It is true that scaling down of the test layout, such as was done in this investigation, results in air-flow Reynolds numbers which are very much smaller than those obtained in the full-scale event so that viscous effects would not be similar. Reference 8 shows, however, that the influence of Reynolds number on wave-diffraction phenomena was small in the case of a sharp-edged body in a shock tube. This information indicates that any changes in flow about the body with Reynolds number had little effect on the incident-shock pattern. Furthermore, in view of the small effects on overall shock strength measured due to a rather extreme surface roughness, it is doubtful if a Reynolds number effect would be significant with regard to this wave parameter. The local air-flow characteristics about the roughness elements might be more noticeably influenced by Reynolds number, however, so that, if such detailed observations could be made in small-scale layouts, the flow might not be similar to that in larger scale layouts. This fact might be true particularly for rounded or smoothly faired bodies where flow separation is not fixed by the geometry as much as it is fixed for sharp-edged bodies.

The Mach stem results which are plotted in figures 15 to 17 have been examined in the light of a possible geometrical similarity of the triple-point path for different heights of burst. Although there is no theoretical justification for similarity based on the parameters d_o, h_c, and α_e, in references 1 and 7 the results were plotted in the form ϕ against $\alpha - \alpha_e$ in which a single curve was considered to be

representative of all the data. In figure 20, all the Mach stem data obtained in this investigation have been plotted in the same form as in references 1 and 7, and the result can be seen to be still quite dependent upon the height of burst. The data of references 1 and 7 are also plotted for comparison, and the reference data also show some dependence upon height of burst rather than appearing as a random scatter of data about a single curve.

The most similarity of the Mach stem data for various heights of burst which was obtained herein was found when plotted in the form shown in figure 21, where $\frac{d_y - d_o}{d_o}$ is plotted against the Mach stem height h_y. While the data have not been reduced to a single curve, there is somehwat less dependence on h_c than appears in figure 20. The data of references 1 and 7 are also shown for comparison in figure 21, and the dependence on height of burst is again apparent here, but to a lesser extent.

CONCLUSIONS

Measurements of peak overpressure and Mach stem height have been made for spherical shock waves moving over smooth and rough surfaces at four different charge heights. The data were obtained on a small-scale test layout with 15-gram pentolite charges and instrumentation capable of directly observing the shock movement with time. The following conclusions may be drawn from examination of the data and comparison with reference data:

1. Good similarity of the relationship between free-air shock peak overpressure and distance with larger scale data was found to exist.

2. The net effect of extreme surface roughness on the relationship of shock peak overpressure at the surface against distance for all heights of burst was to lower the overpressures slightly.

3. The effect of extreme surface roughness on the Mach stem formation point was to delay the formation at the greatest charge height $(6.25\ \text{ft/lb}^{1/3})$.

4. The effect of extreme surface roughness on the growth of the Mach stem with horizontal distance was to lower the Mach stem height at all heights of burst.

The data did not fit a geometrical similarity parameter for the path of the triple point at different heights of burst as suggested by other investigators. A simple similarity parameter $\frac{d_y - d_o}{d_o}$ was found which showed only a small influence of burst height on the path of the triple point.

Langley Aeronautical Laboratory,
National Advisory Committee for Aeronautics,
Langley Field, Va., January 21, 1955.

REFERENCES

1. Bryant, E. J., Eberhard, R. A., and Kingery, C. N.: Mach Reflection Over Hard Packed Dirt and Dry Sand. Rep. No. 809, Ballistic Res. Lab., Aberdeen Proving Ground, July 1952.

2. Eberhard, R. A., Stoering, J. P., and Coulter, G.: Effect of Solid Walls on the Mach Region. Rep. No. 759, Ballistic Res. Lab., Aberdeen Proving Ground, May 1951.

3. Curtis, Wesley: Free Air Blast Measurements on Spherical Pentolite. Memo. Rep. No. 544, Ballistic Res. Lab., Aberdeen Proving Ground, July 1951.

4. Hartmann, G. K., and Kalavski, P. Z.: The Optimum Height of Burst for High Explosives. NAVORD Rep. No. 2451, U. S. Naval Ord. Lab., (White Oak, Md.), July 21, 1952.

5. Taub, A. H.: The Effect of Height of Burst on the Blast From Explosives. NDRC Rep. No. A-486 (OSRD Rep. No. 6660), Div. 2, Mar. 1946.

6. Stoner, R. G.: Mach Reflection of Shock Waves From Charges Detonated in Air. Study of Shock Waves (Project OD-03). Vol. 3, Air and Earth Shock, NDRC Monthly Rep. AES-3 (OSRD No. 4257), Div. 2, Oct. 25, 1944, pp. 17-37.

7. Halverson, R. R.: The Effect of Air Burst on the Blast From Bombs and Small Charges - II. Analysis of Experimental Results. NDRC Rep. No. A-320 (OSRD Rep. No. 4899), Div. 2, Apr. 6, 1945.

8. Griffith, W. C., Weimer, D. K., Brickl, D. E., and Bleakney, Walker: The Effect of Reynolds Number on the Diffraction of a Shock Wave. Tech. Rep. II - 8 (Contract N6 ori-105 Task II), Princeton Univ., Dept. of Phys., Feb. 1951.

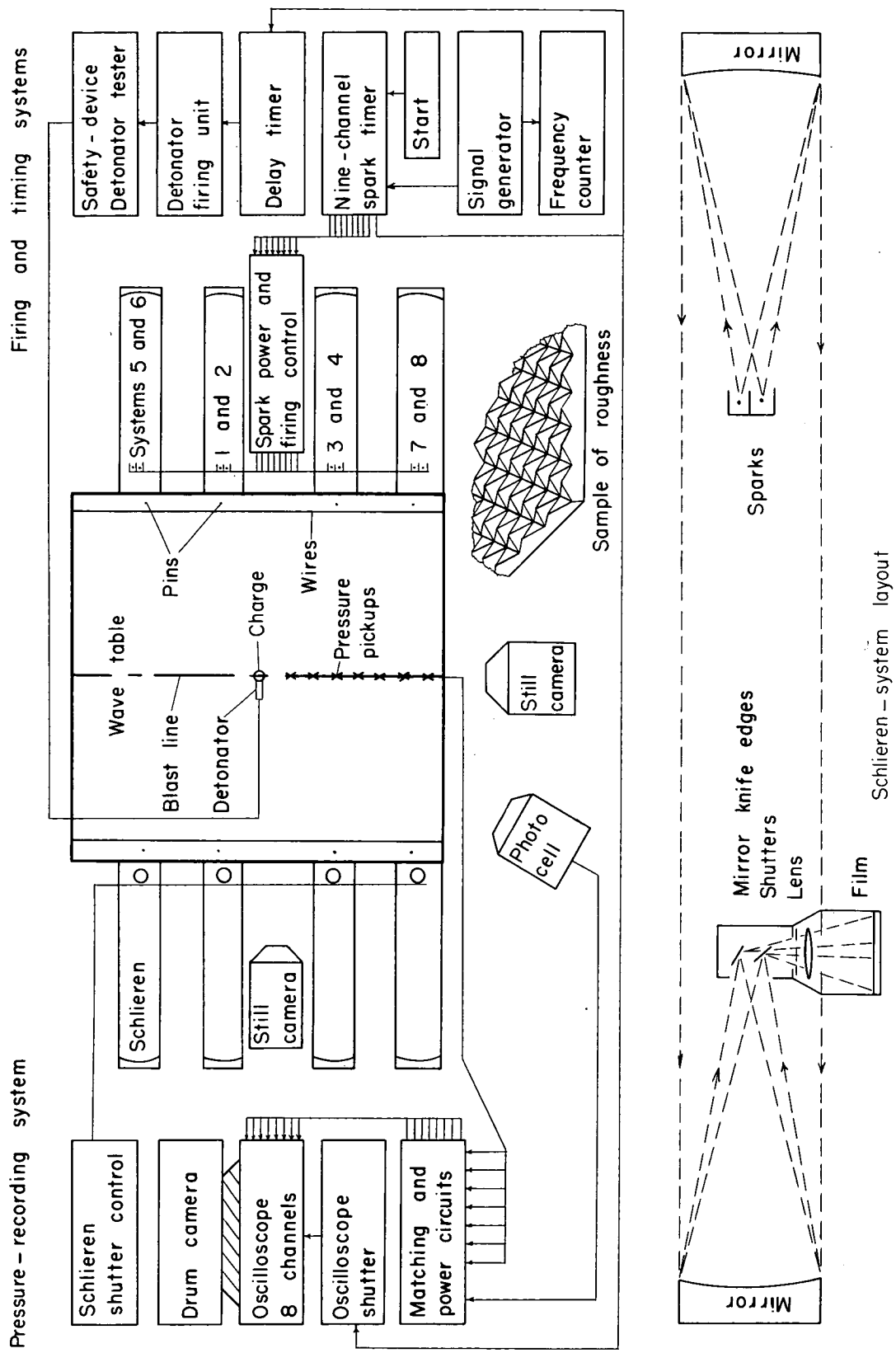

Figure 1.- Schematic diagram of wave table and instrumentation.

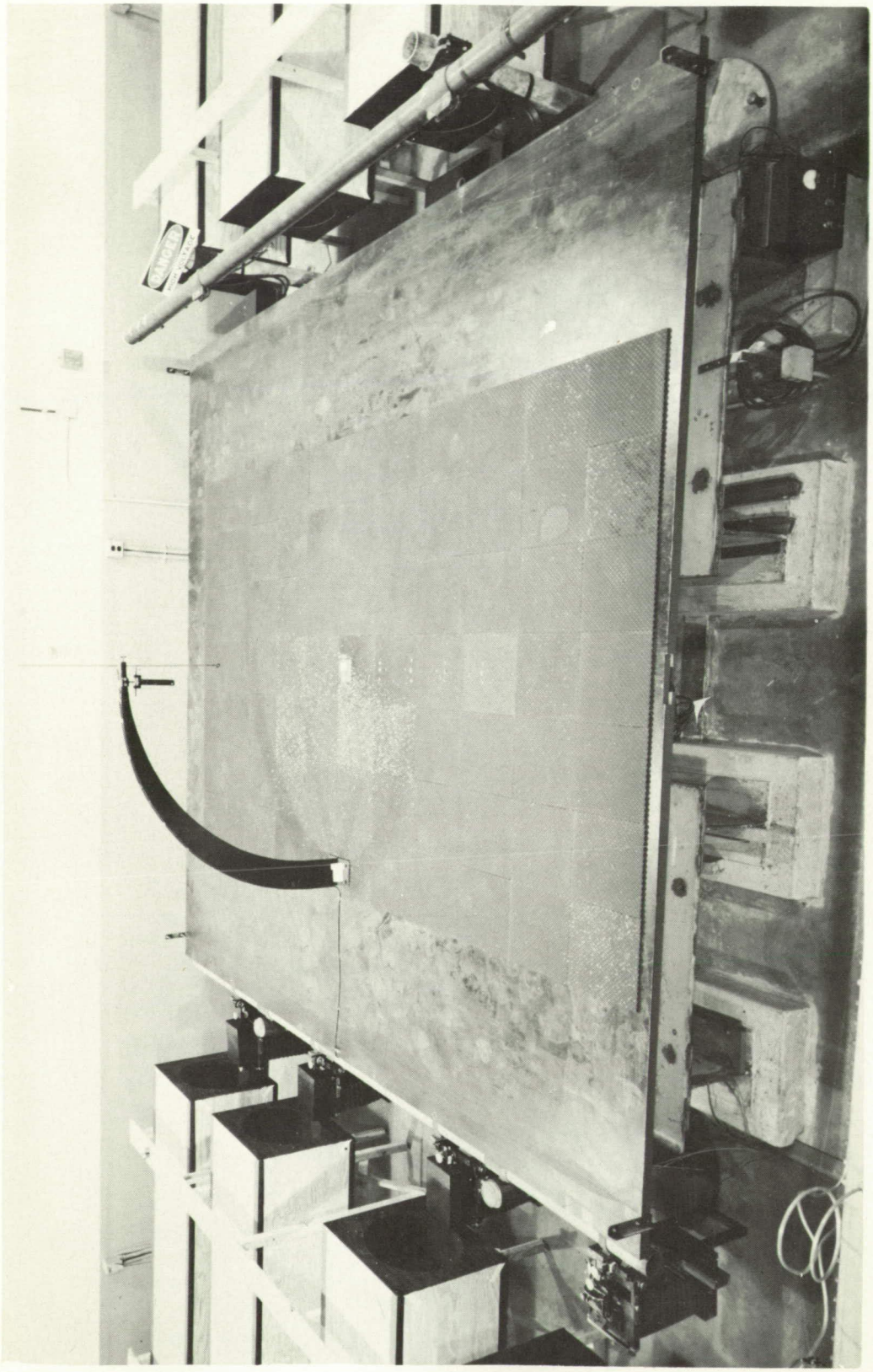

L-87085

(a) With roughness.

Figure 2.- Views of wave table.

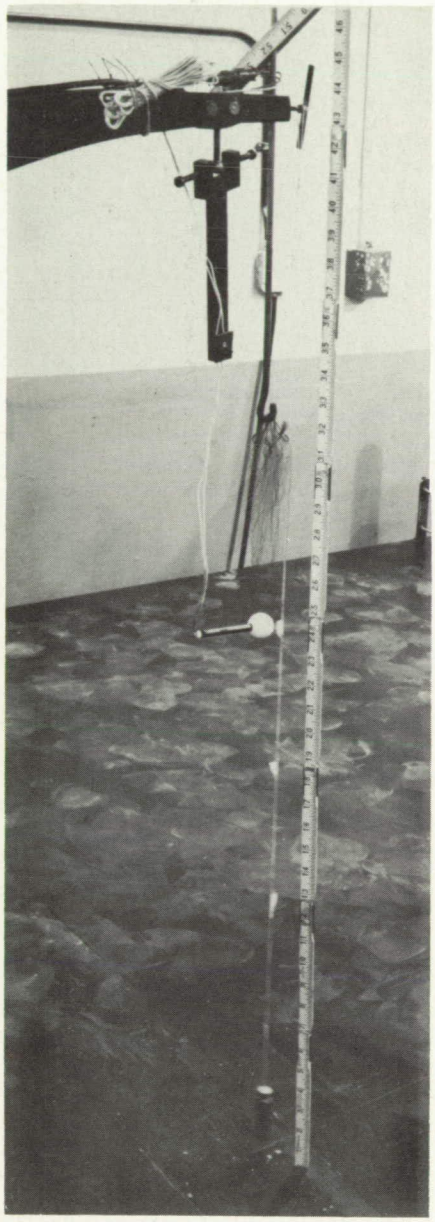

L-87578

(b) Support arm with charge at height of 2 feet.

Figure 2.- Concluded.

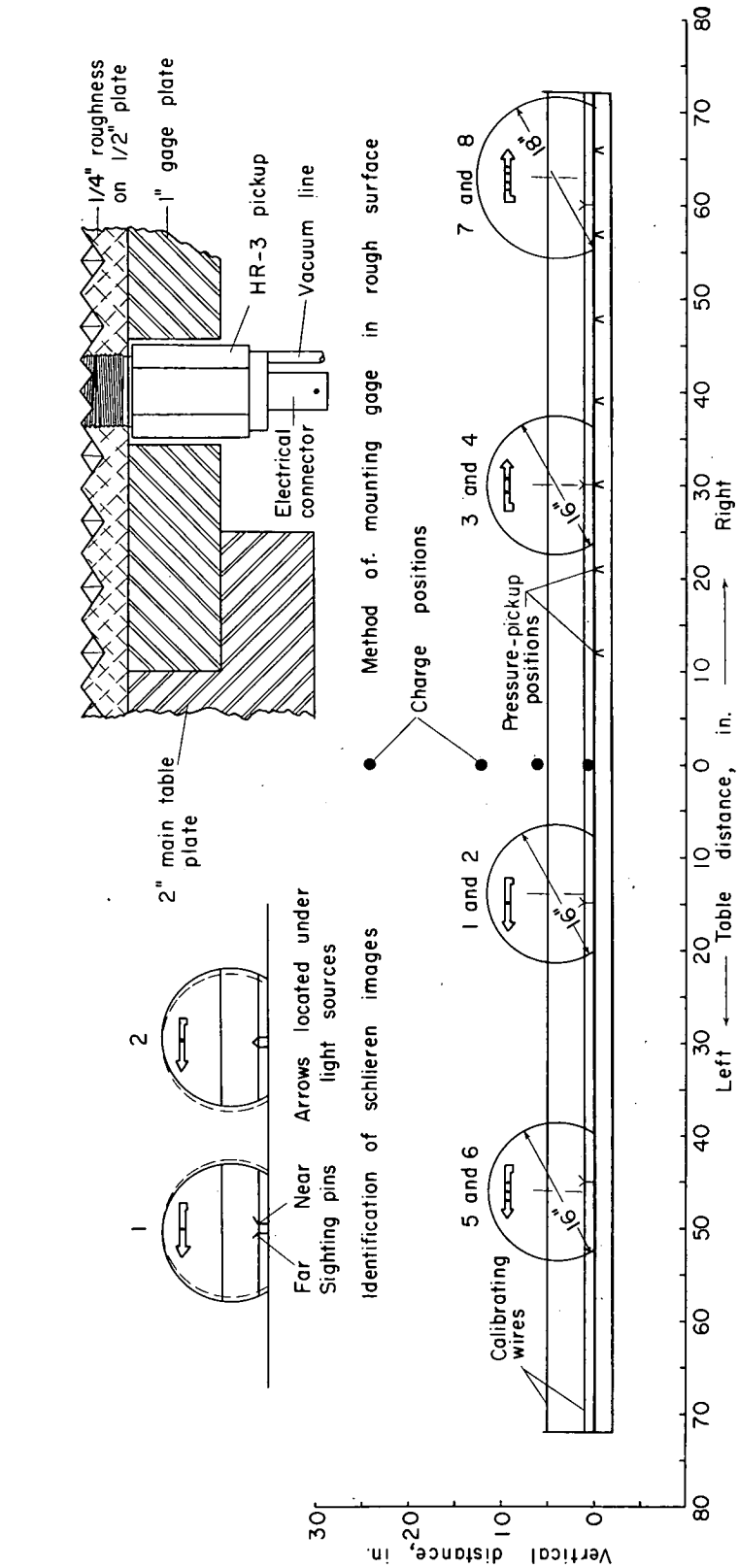

Figure 3.- Sectional view of table along blast line with location of instrumentation.

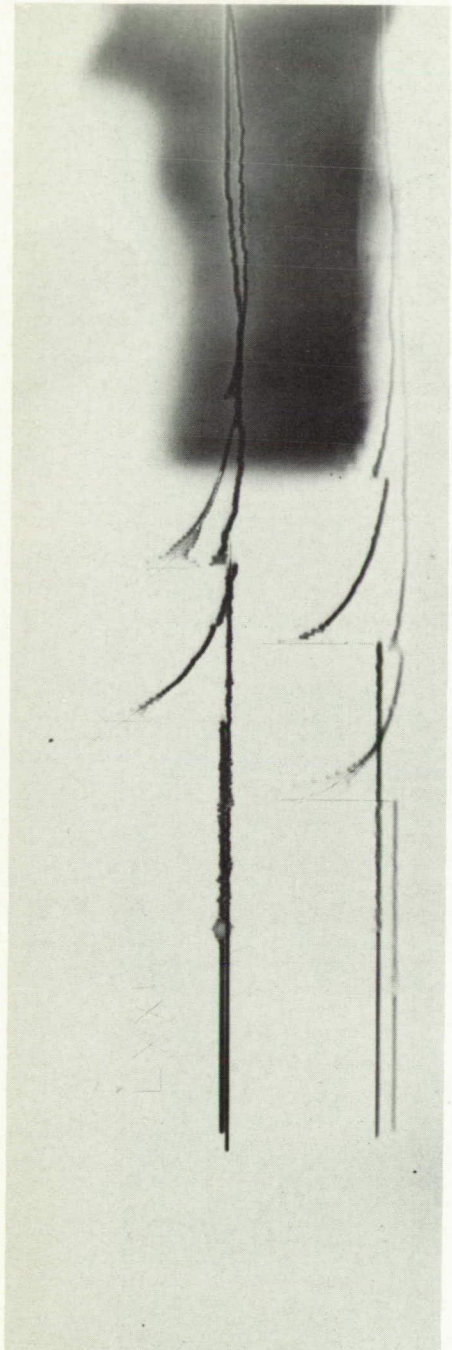

(a) Drum-camera pressure records for smooth surface.

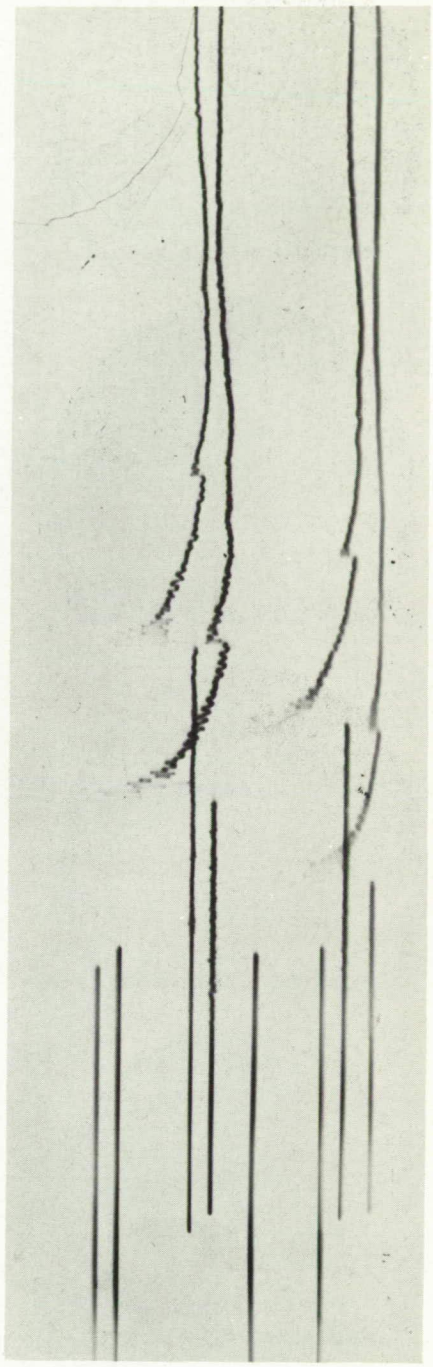

(b) Drum-camera pressure records for rough surface.

Figure 4.- Typical data records at 2-foot charge height.

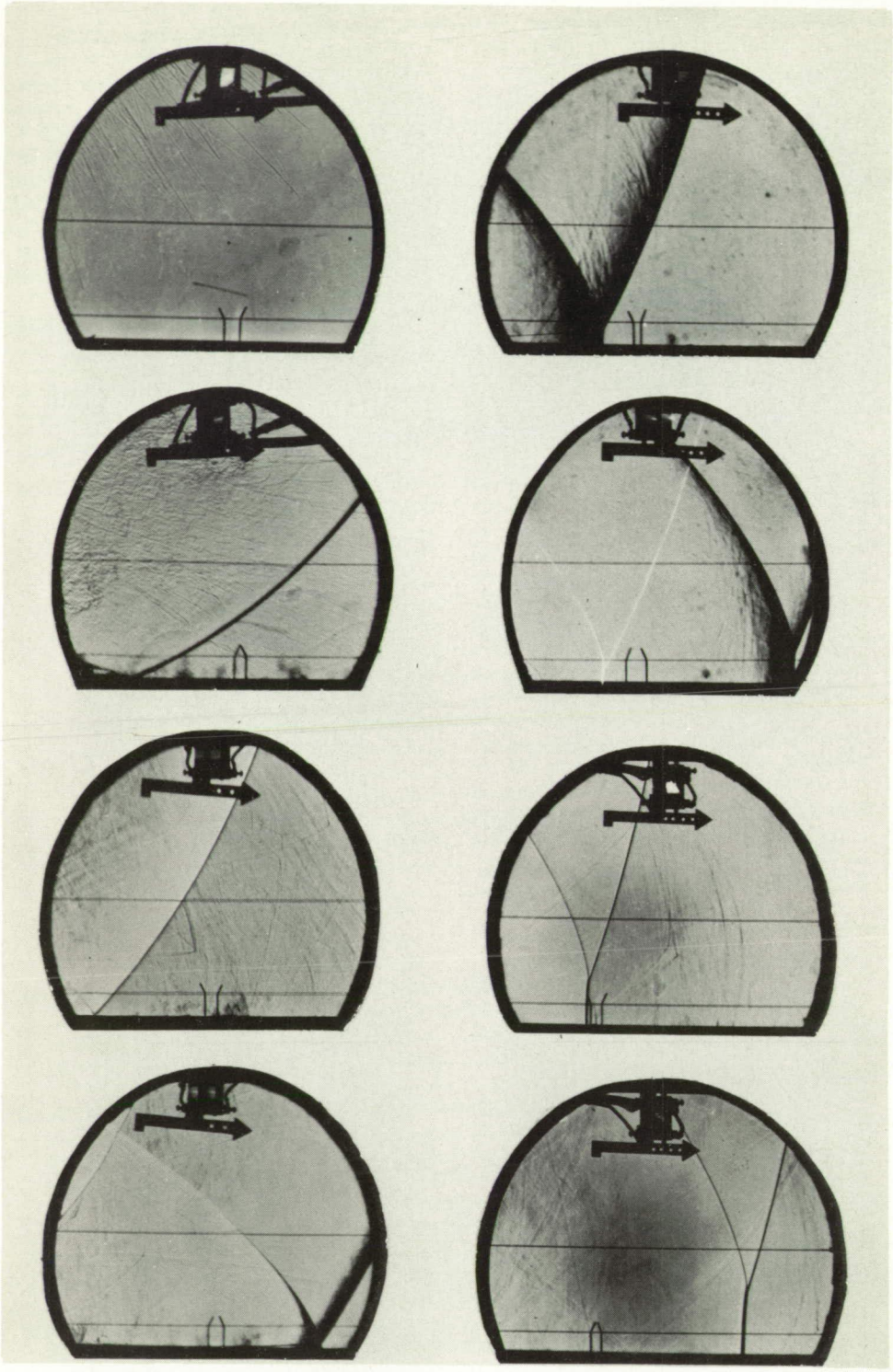

L-87579

(c) Nine-channel schlieren photographs for smooth surface.

Figure 4.- Continued.

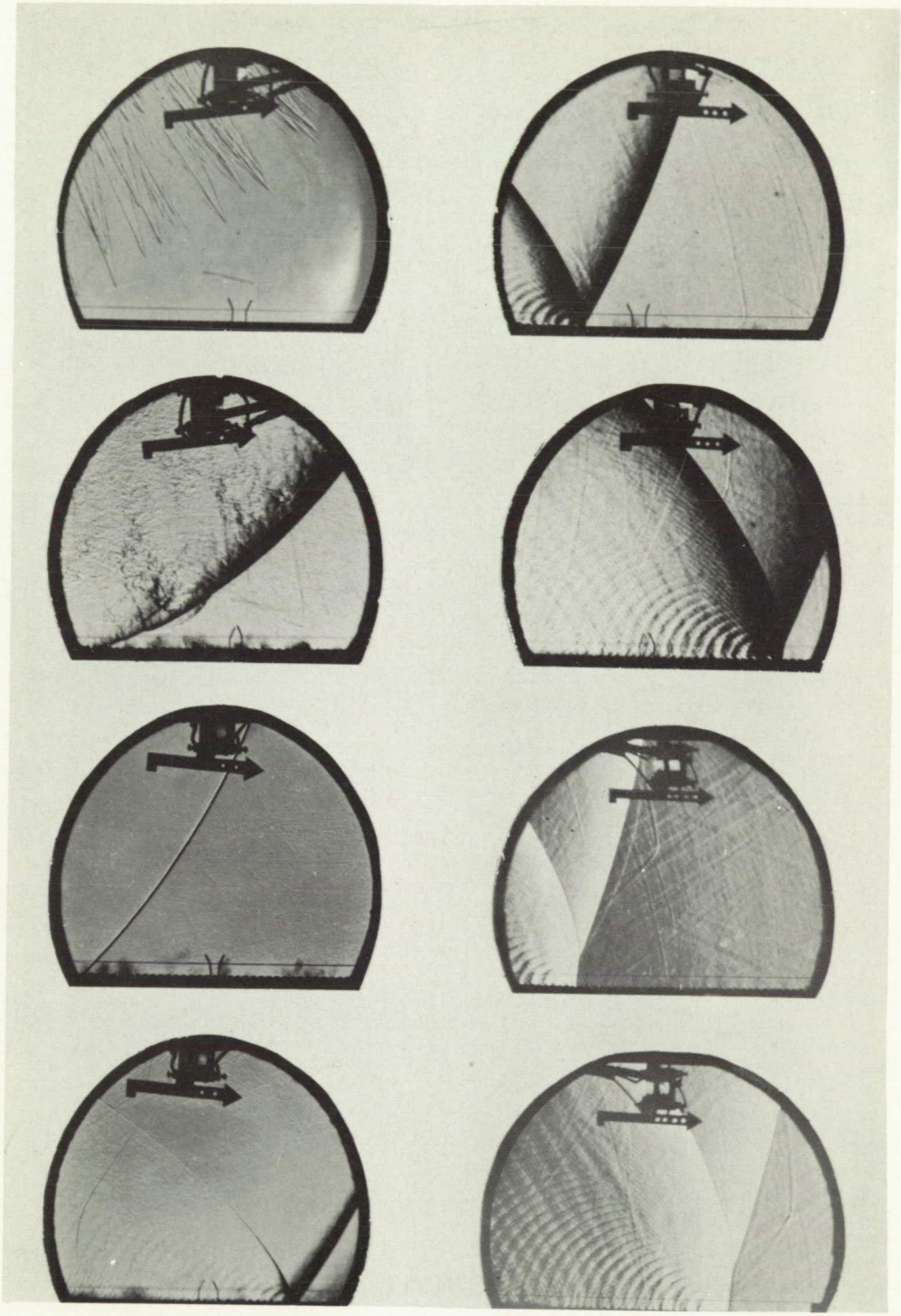

L-87580

(d) Nine-channel schlieren photographs for rough surface.

Figure 4.- Concluded.

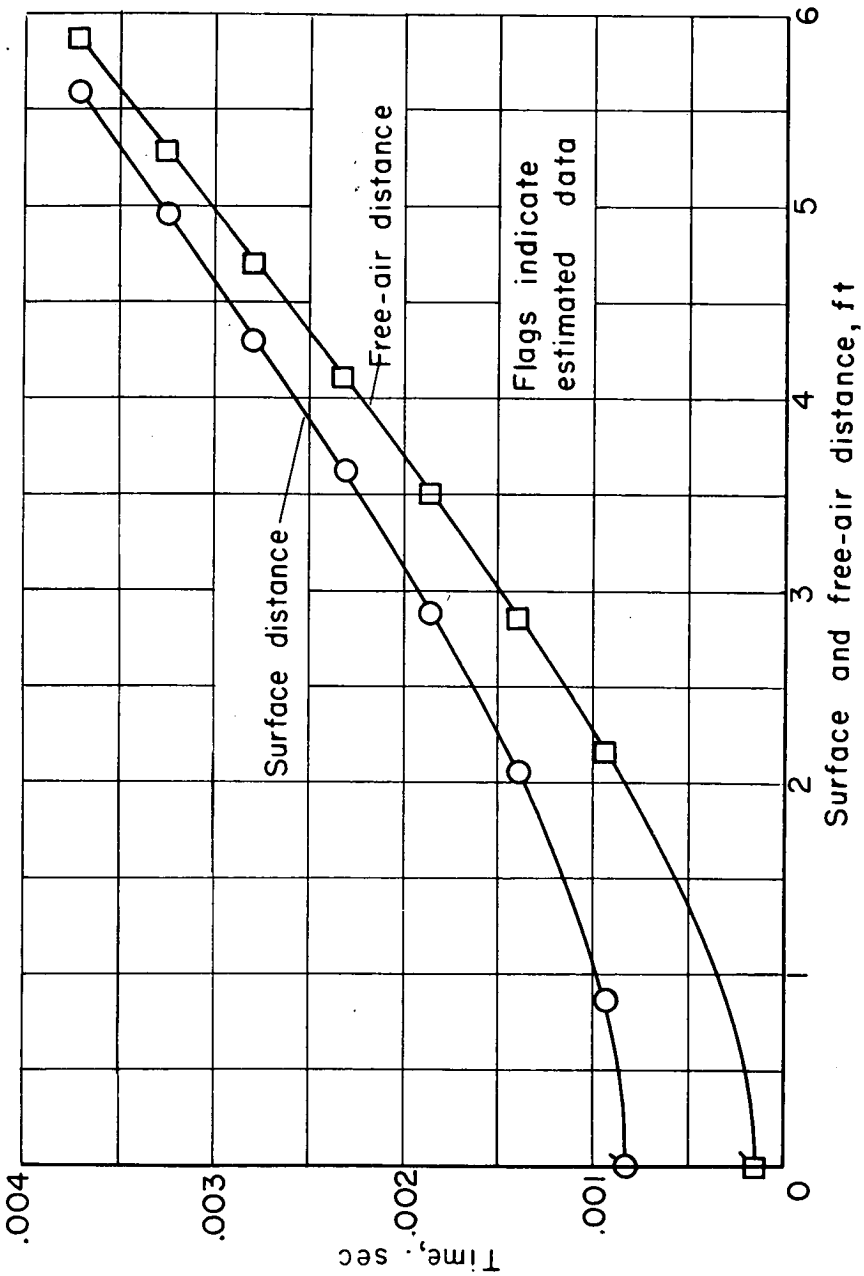

Figure 5.- Typical time-distance history of shock movement along surface and in free air taken from figure 4(c).

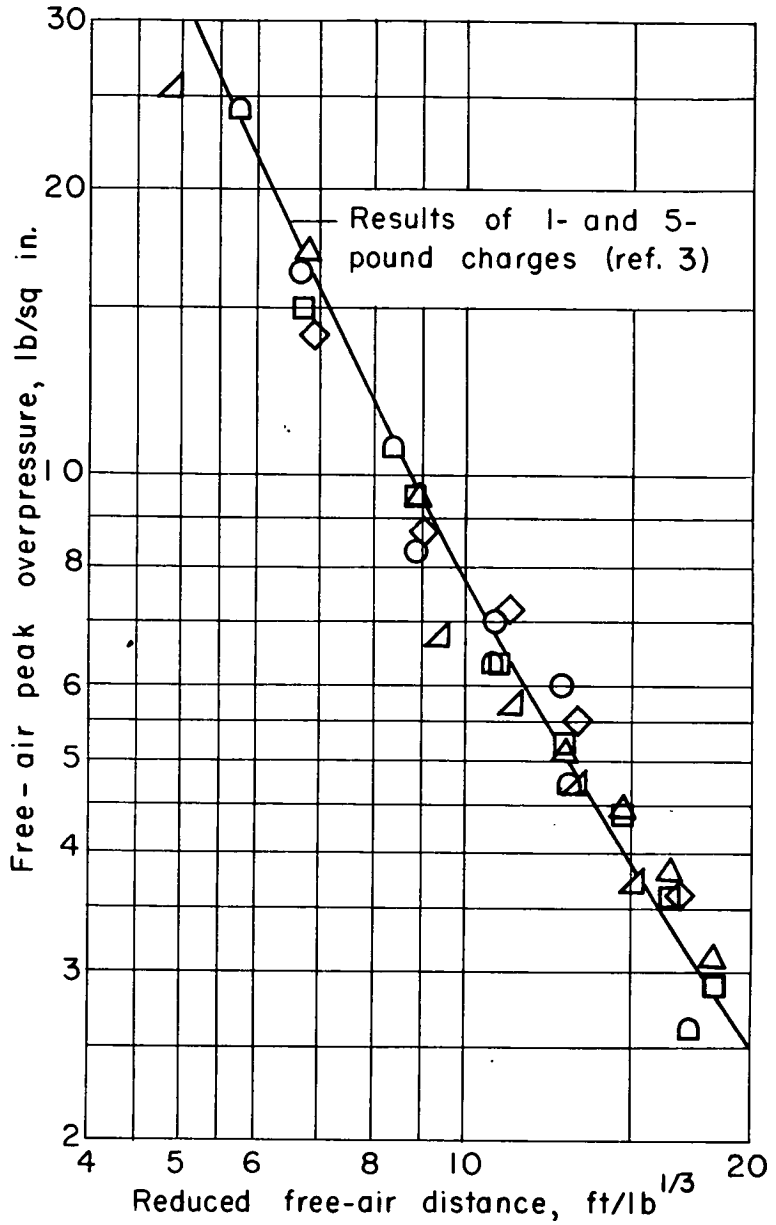

Figure 6.- Free-air pressures obtained from schlieren data; each type symbol represents separate test.

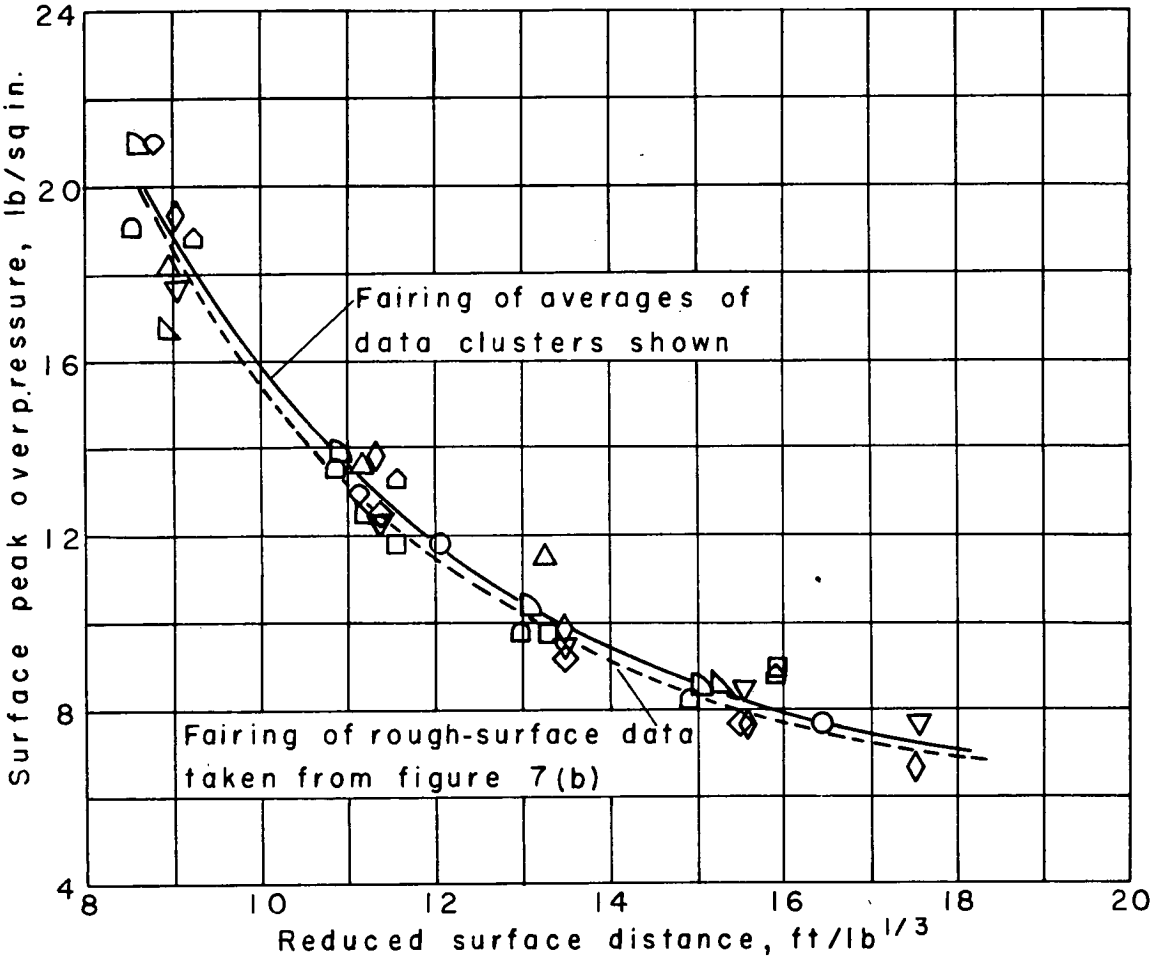

(a) Smooth-surface data; each type symbol represents separate test.

Figure 7.- Surface peak overpressures obtained from schlieren data for 6.25 $ft/lb^{1/3}$ reduced height of burst (2-ft actual charge height).

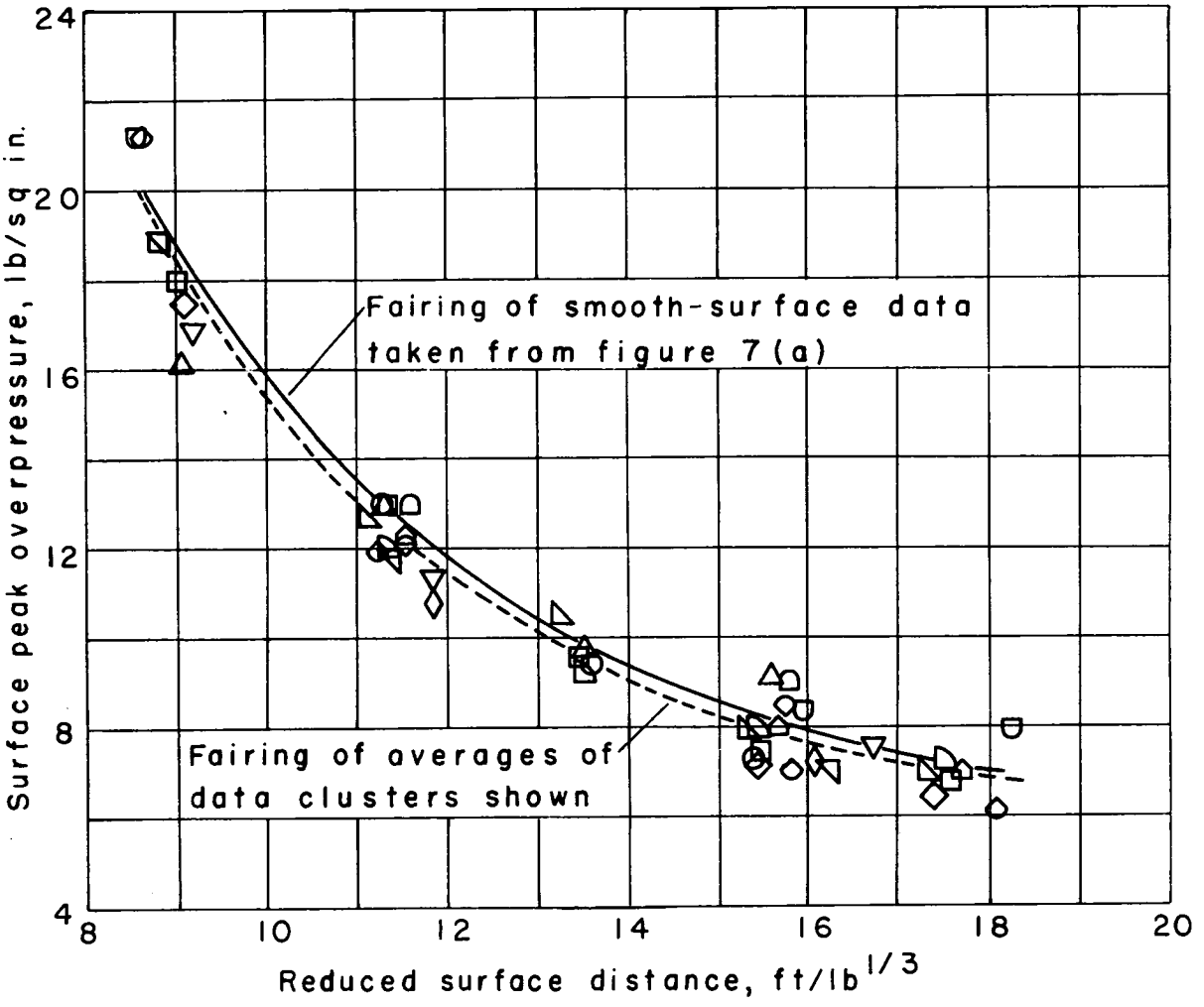

(b) Rough-surface data; each type symbol represents separate test.

Figure 7.- Concluded.

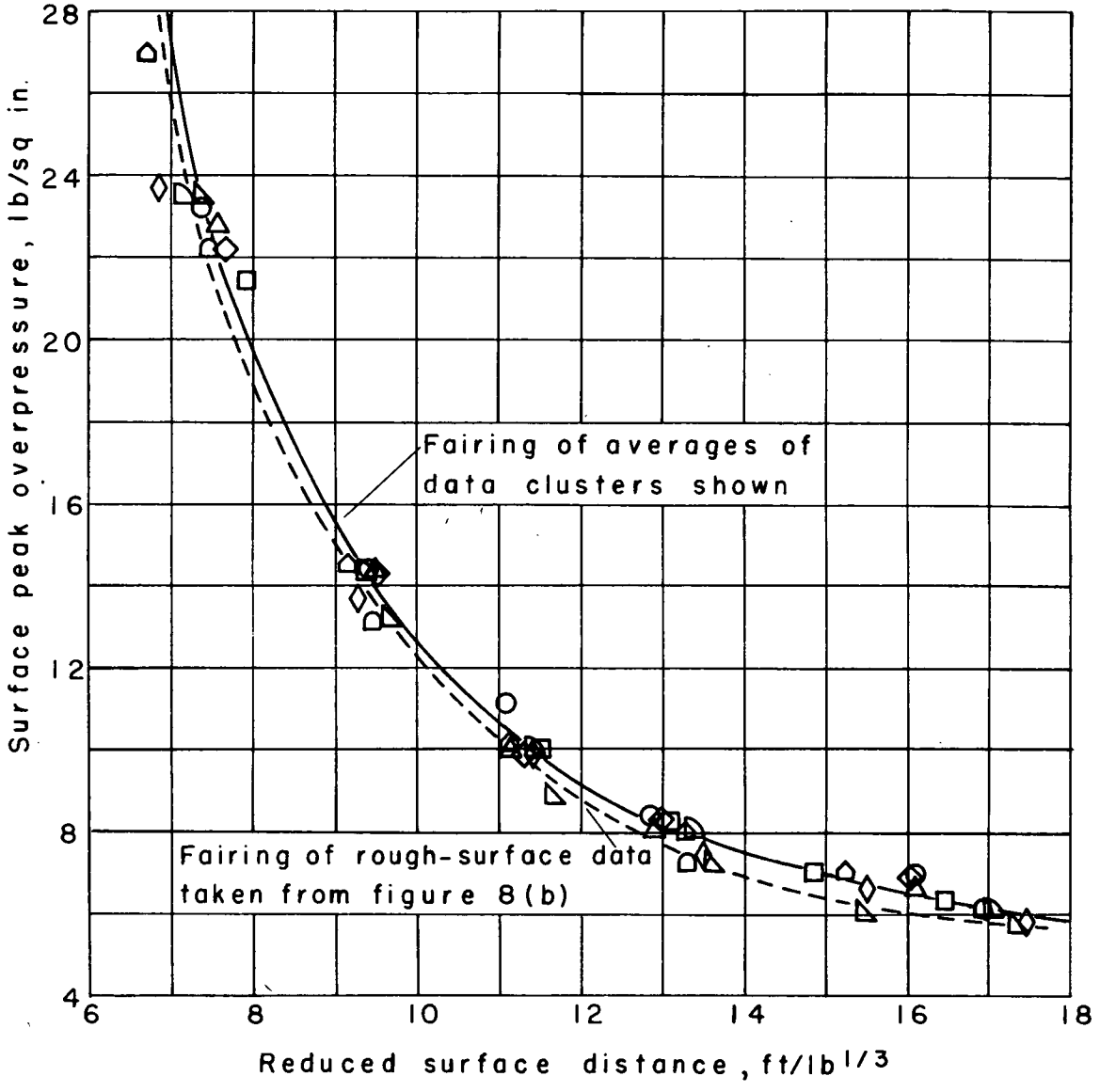

(a) Smooth-surface data; each type symbol represents separate test.

Figure 8.- Surface peak overpressures obtained from schlieren data for 3.125 $ft/lb^{1/3}$ reduced height of burst (1-ft actual charge height).

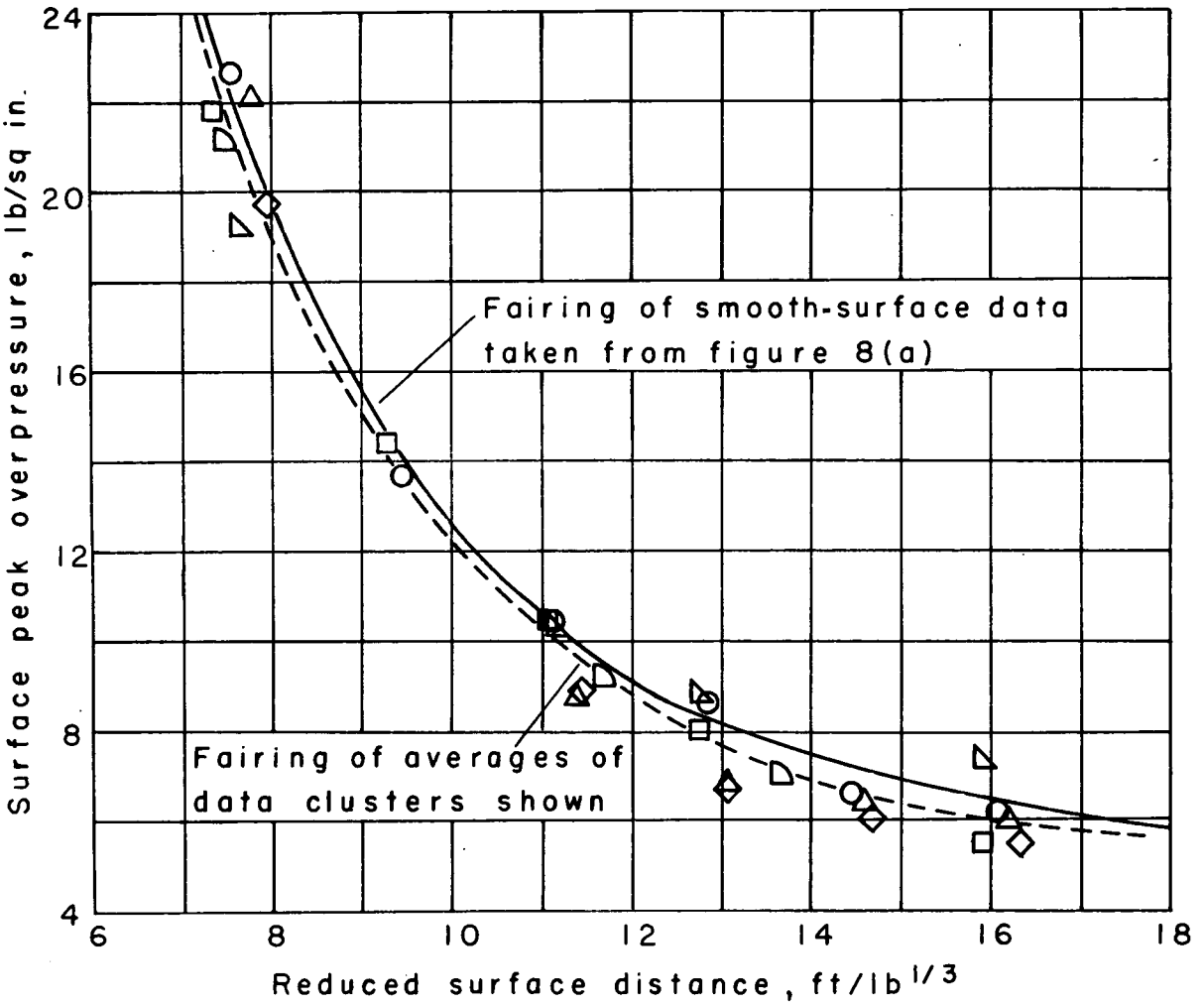

(b) Rough-surface data; each type symbol represents separate test.

Figure 8.- Concluded.

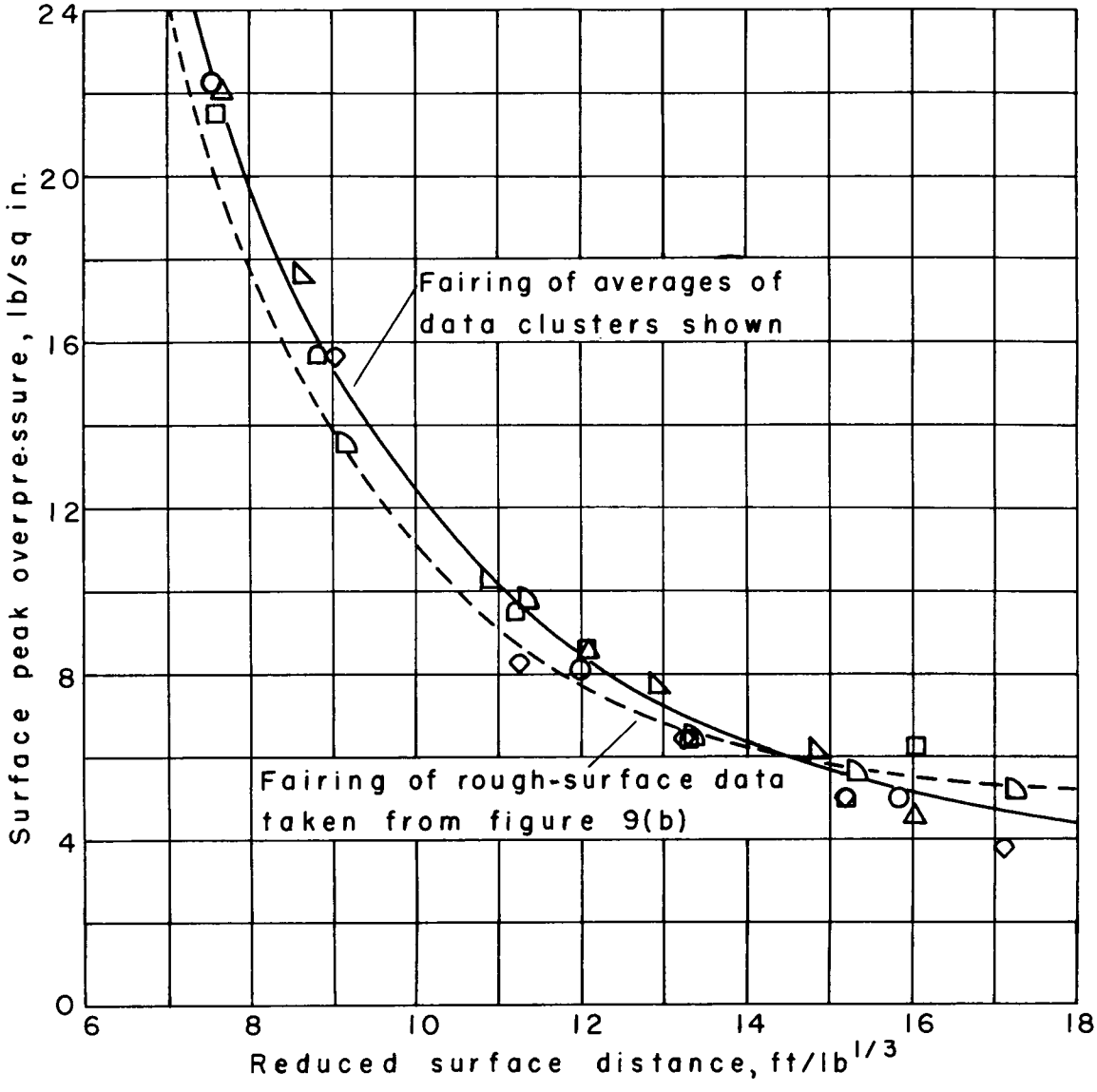

(a) Smooth-surface data; each type symbol represents separate test.

Figure 9.- Surface peak overpressures obtained from schlieren data for 1.56 ft/lb$^{1/3}$ reduced height of burst (6-in. actual charge height).

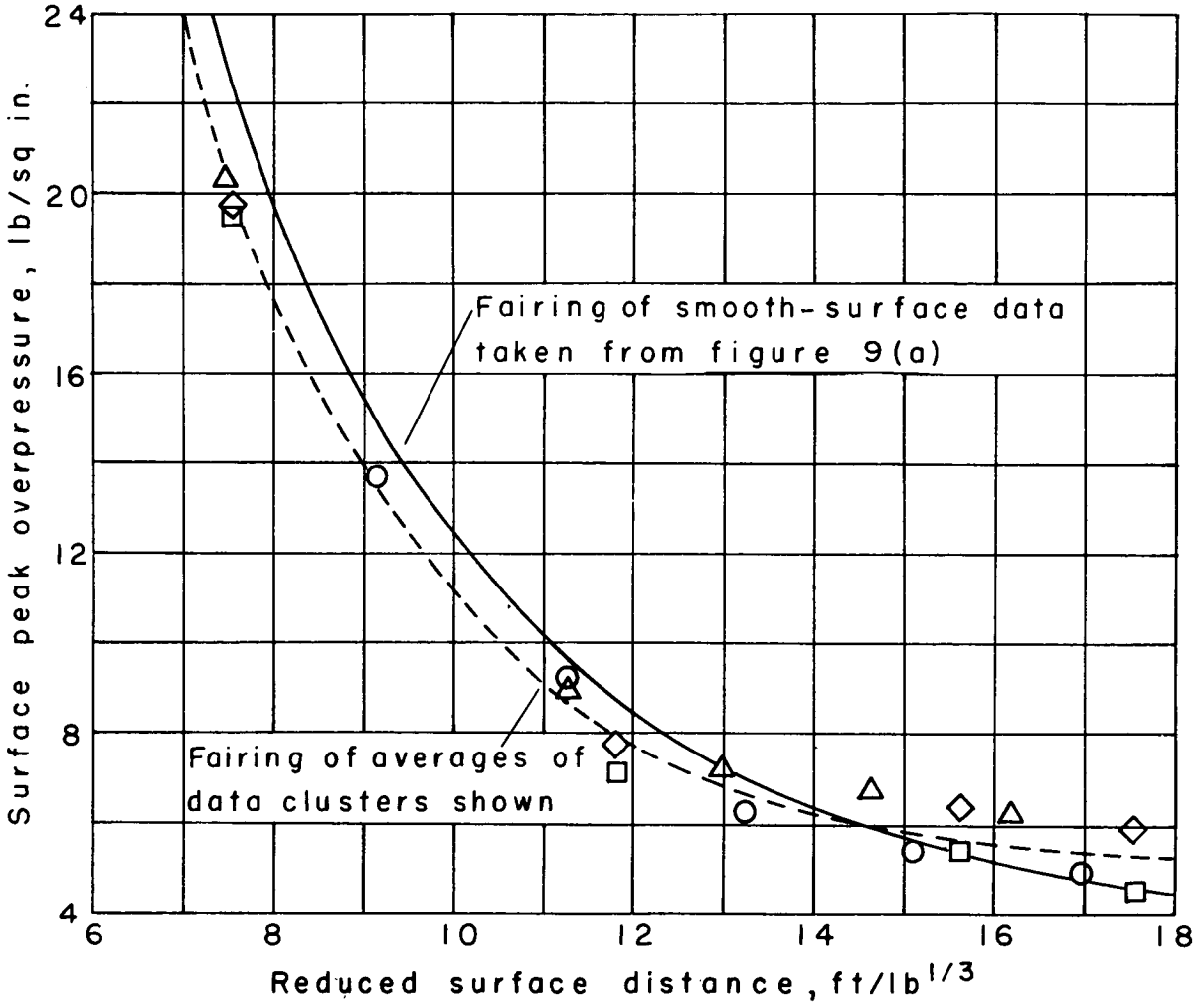

(b) Rough-surface data; each type symbol represents separate test.

Figure 9.- Concluded.

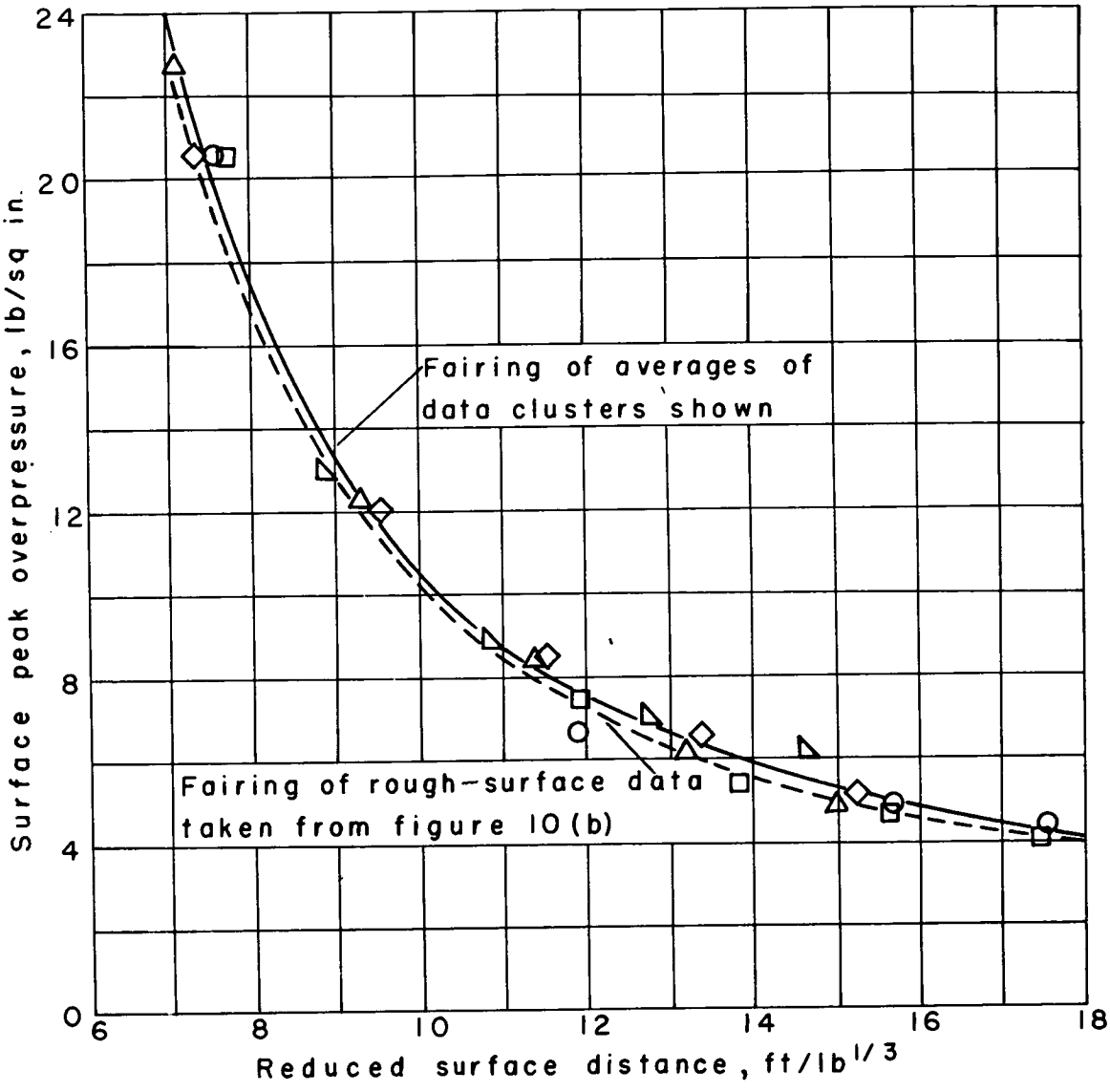

(a) Smooth-surface data; each type symbol represents separate test.

Figure 10.- Surface peak overpressures obtained from schlieren data for 0.13 ft/lb$^{1/3}$ reduced height of burst (0.5-in. actual charge height).

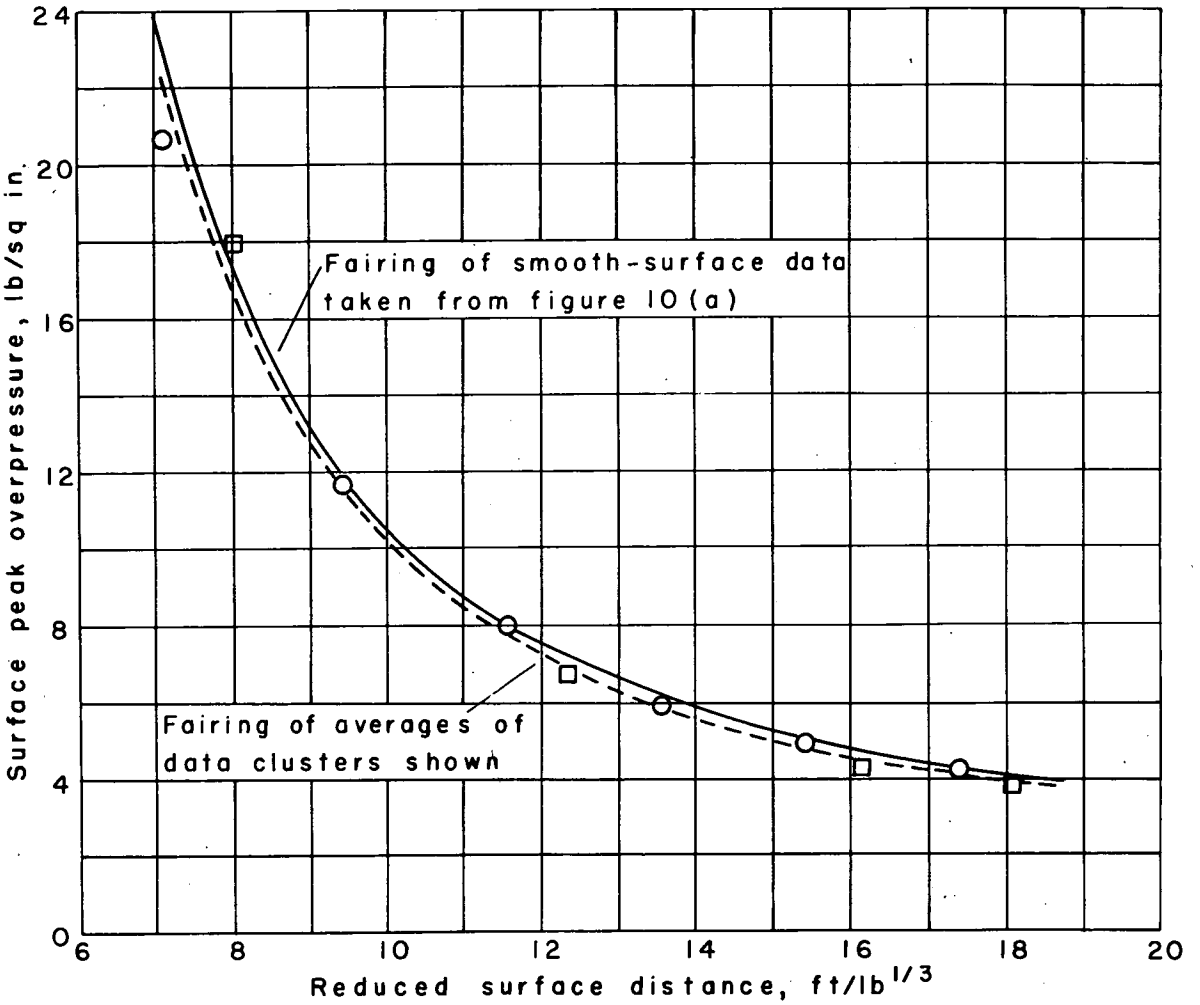

(b) Rough-surface data; each type symbol represents separate test.

Figure 10.- Concluded.

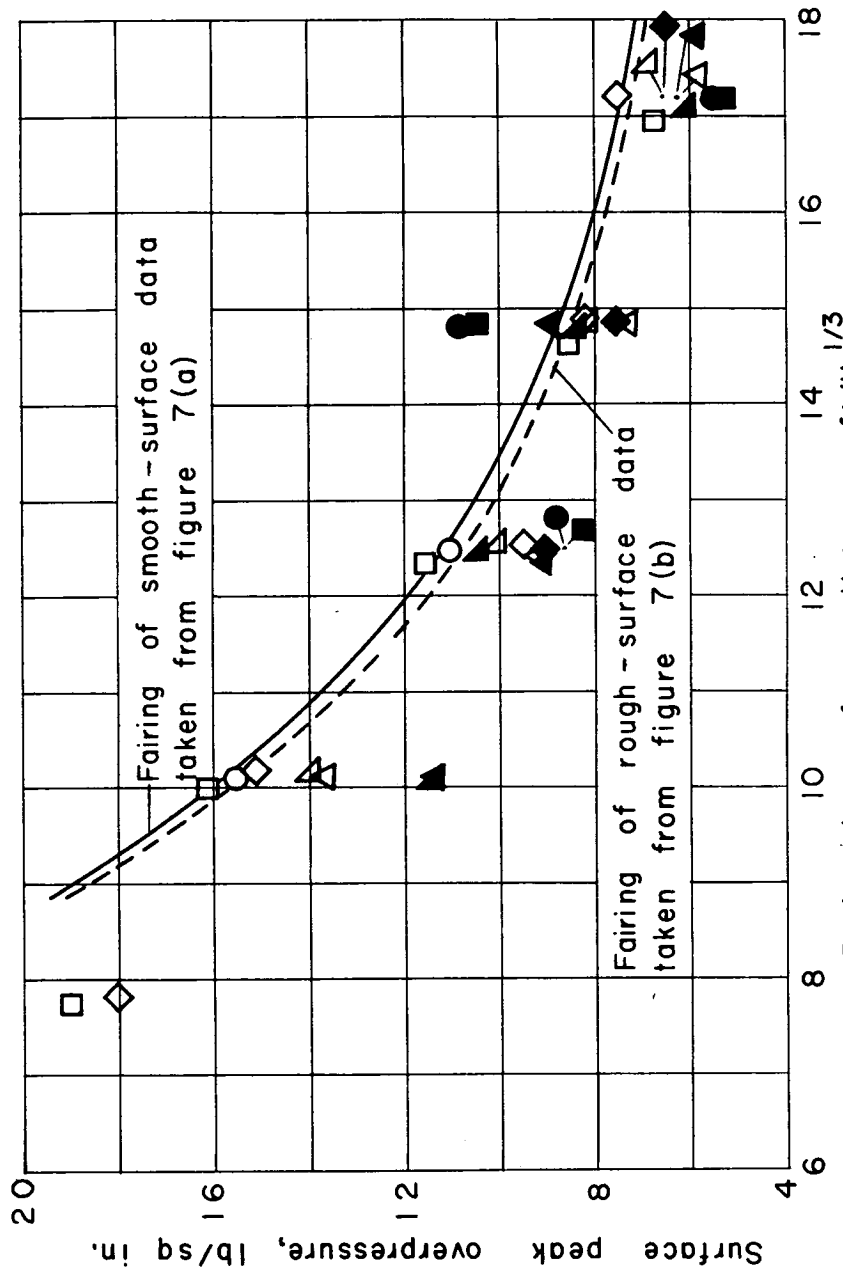

Figure 11.- Comparison of surface peak overpressures obtained from pressure pickups and fairing of schlieren data for 6.25 $ft/lb^{1/3}$ reduced height of burst. Solid symbols represent smooth-surface data; open symbols represent rough-surface data.

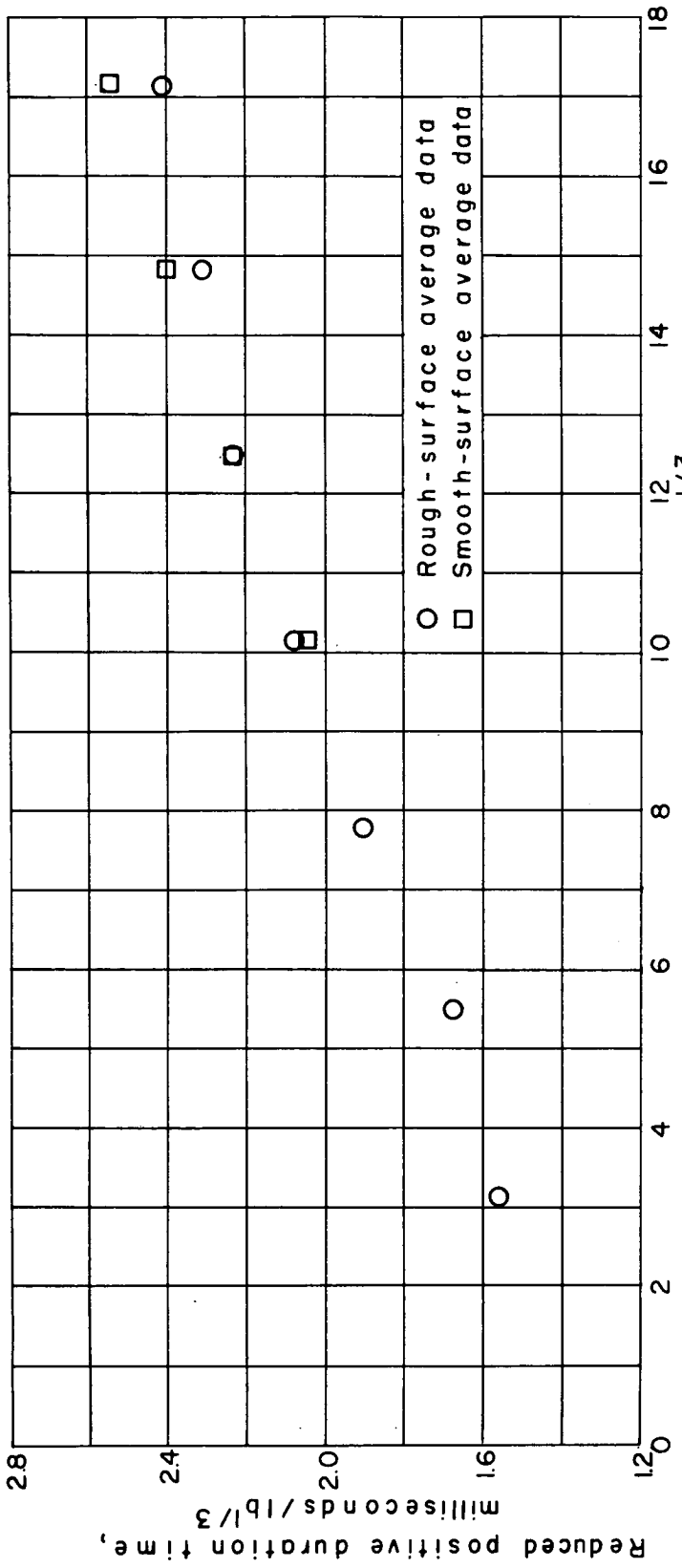

Figure 12.- Comparison of time duration of positive overpressures of smooth- and rough-surface data for 6.25 ft/lb$^{1/3}$ reduced height of burst.

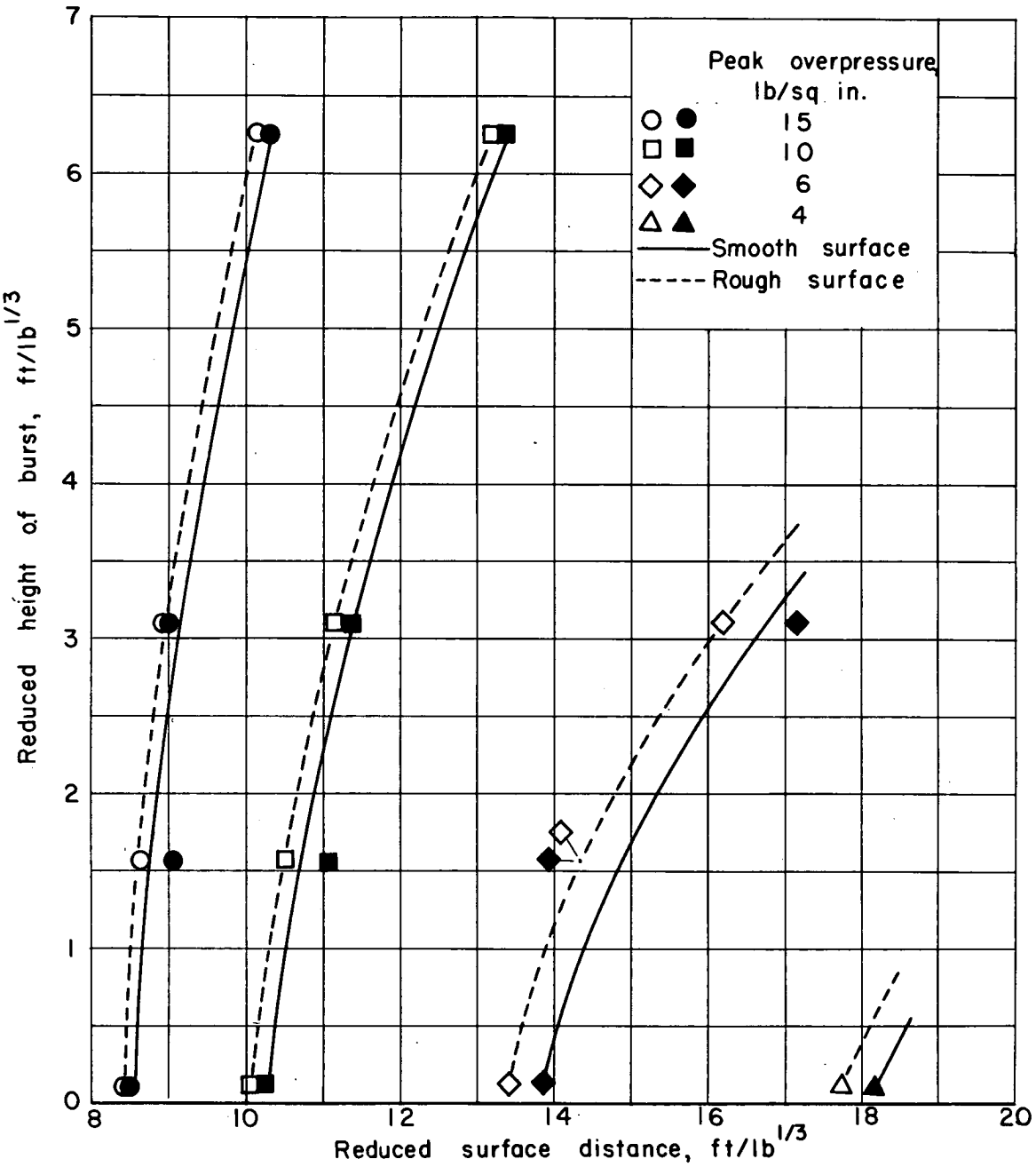

Figure 13.- Comparison of effect of height of burst on peak overpressure over smooth and rough surfaces. Solid and open symbols represent points taken from faired curves of smooth and rough data of figures 7 to 10.

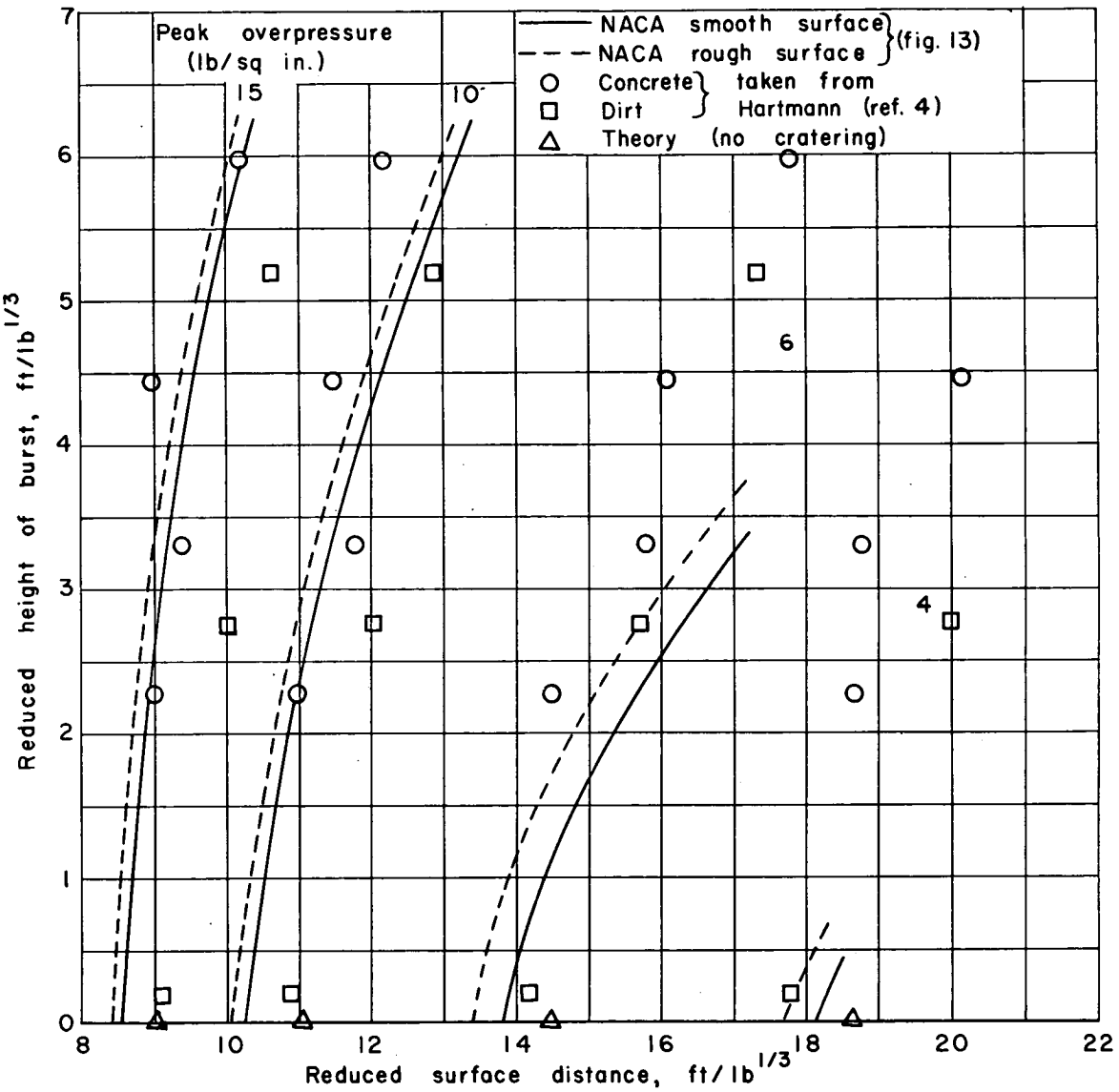

Figure 14.- Comparison of height-of-burst curves of smooth and rough surfaces with reference data.

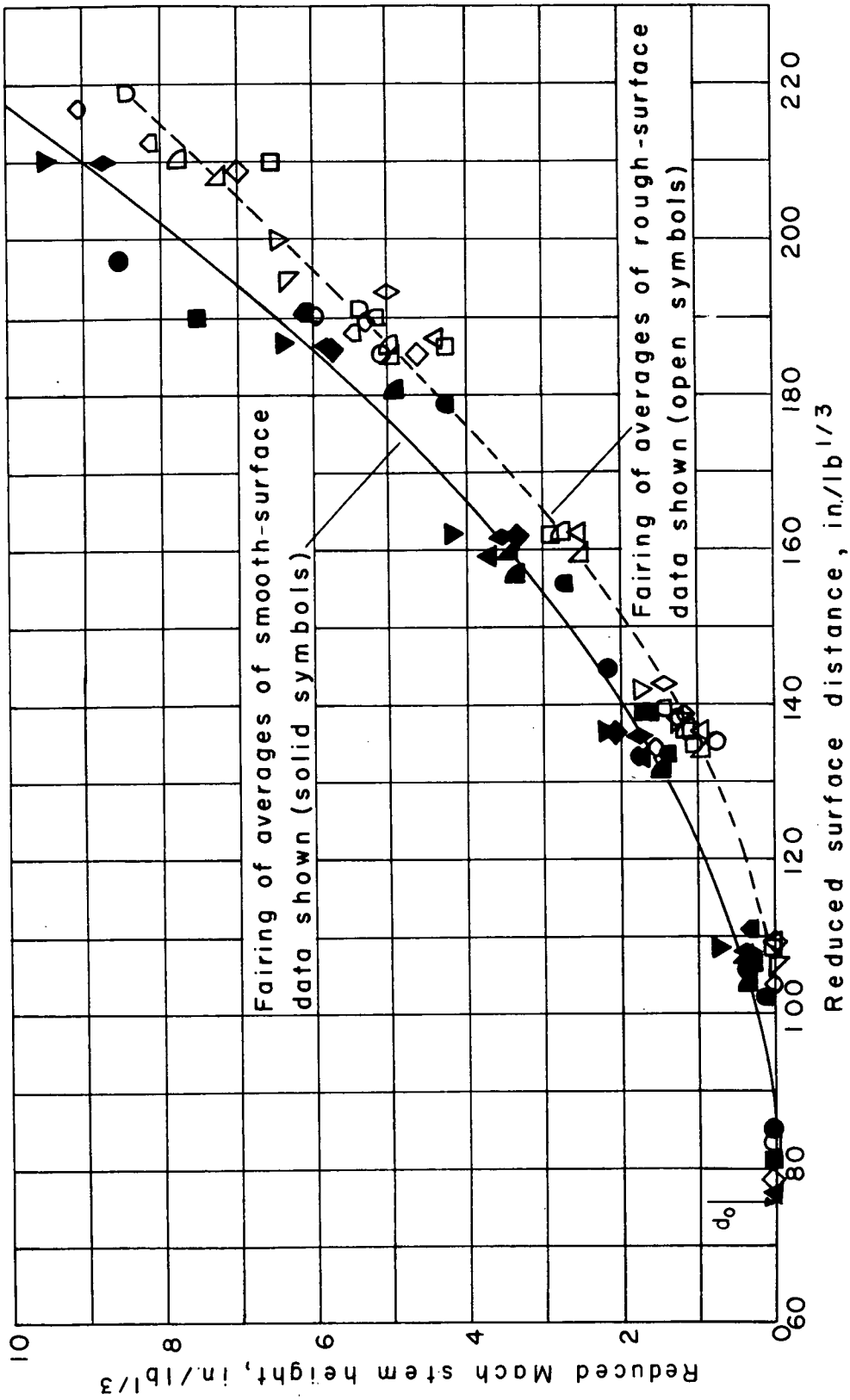

Figure 15.- Comparison of Mach stem growth over smooth and rough surfaces for 6.25 ft/lb$^{1/3}$ reduced height of burst; each type symbol represents separate test.

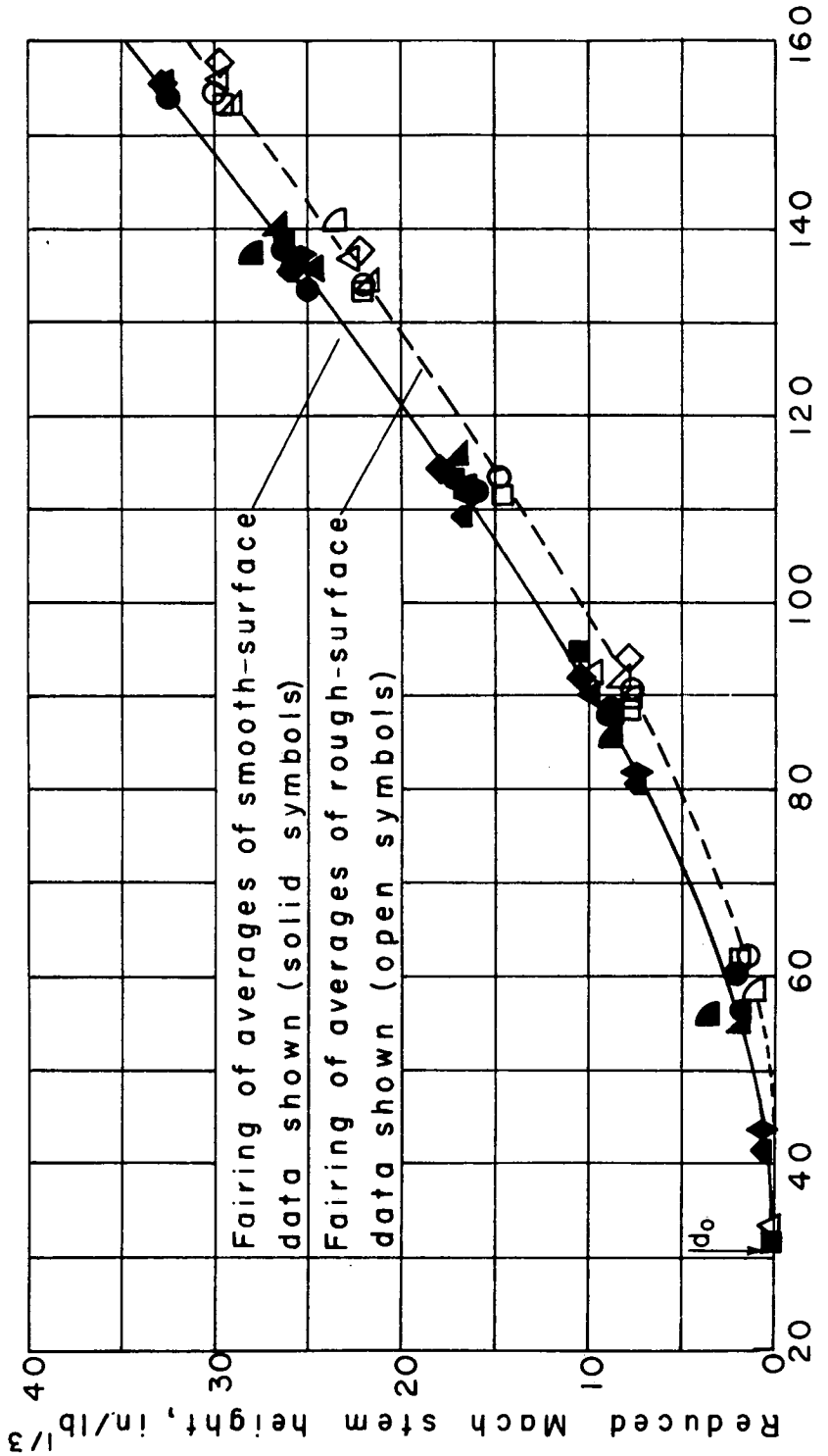

Figure 16.- Comparison of Mach stem growth over smooth and rough surfaces for 3.125 ft/lb$^{1/3}$ reduced height of burst; each type symbol represents separate test.

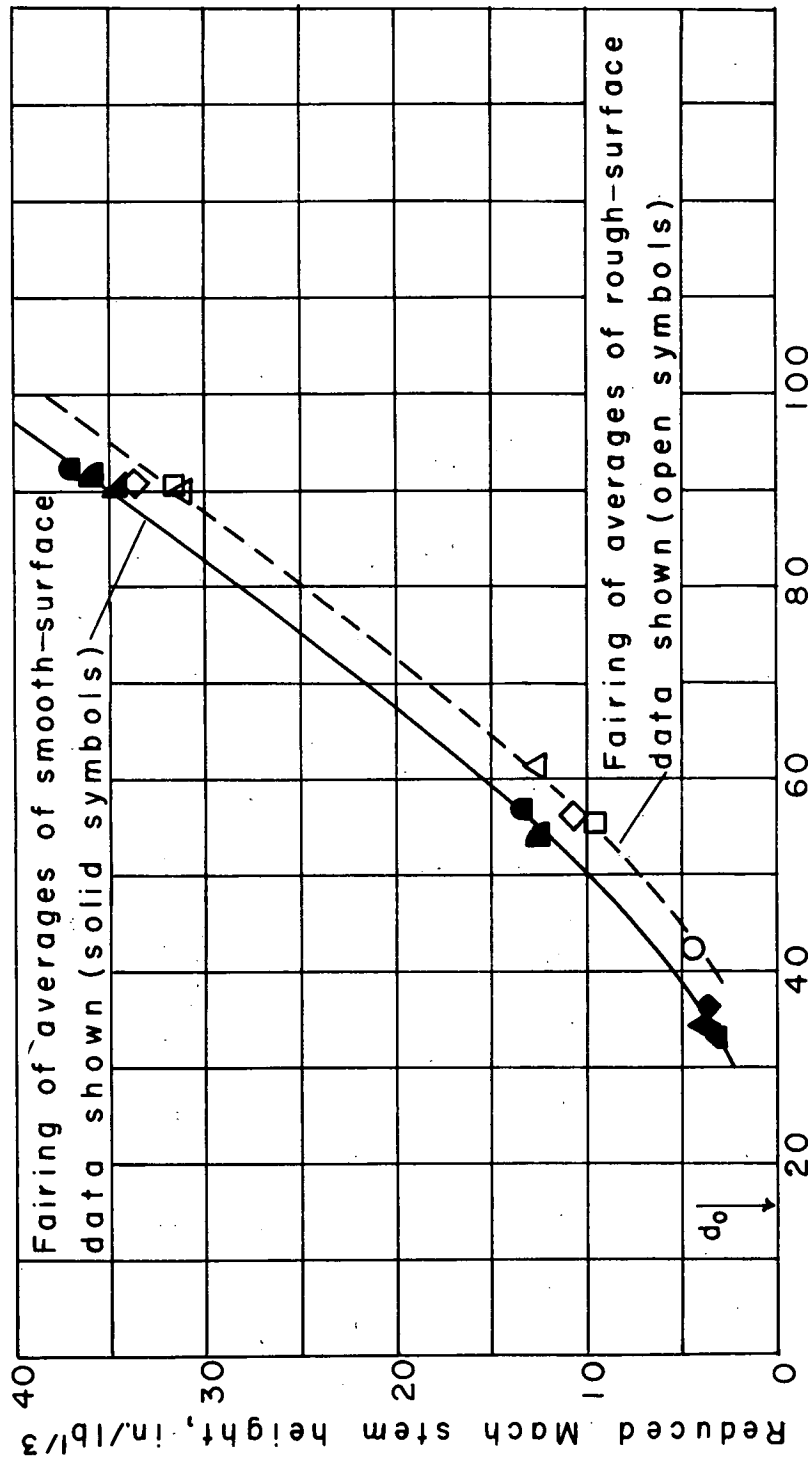

Figure 17.- Comparison of Mach stem growth over smooth and rough surfaces for 1.56 $ft/lb^{1/3}$ reduced height of burst; each type symbol represents separate test.

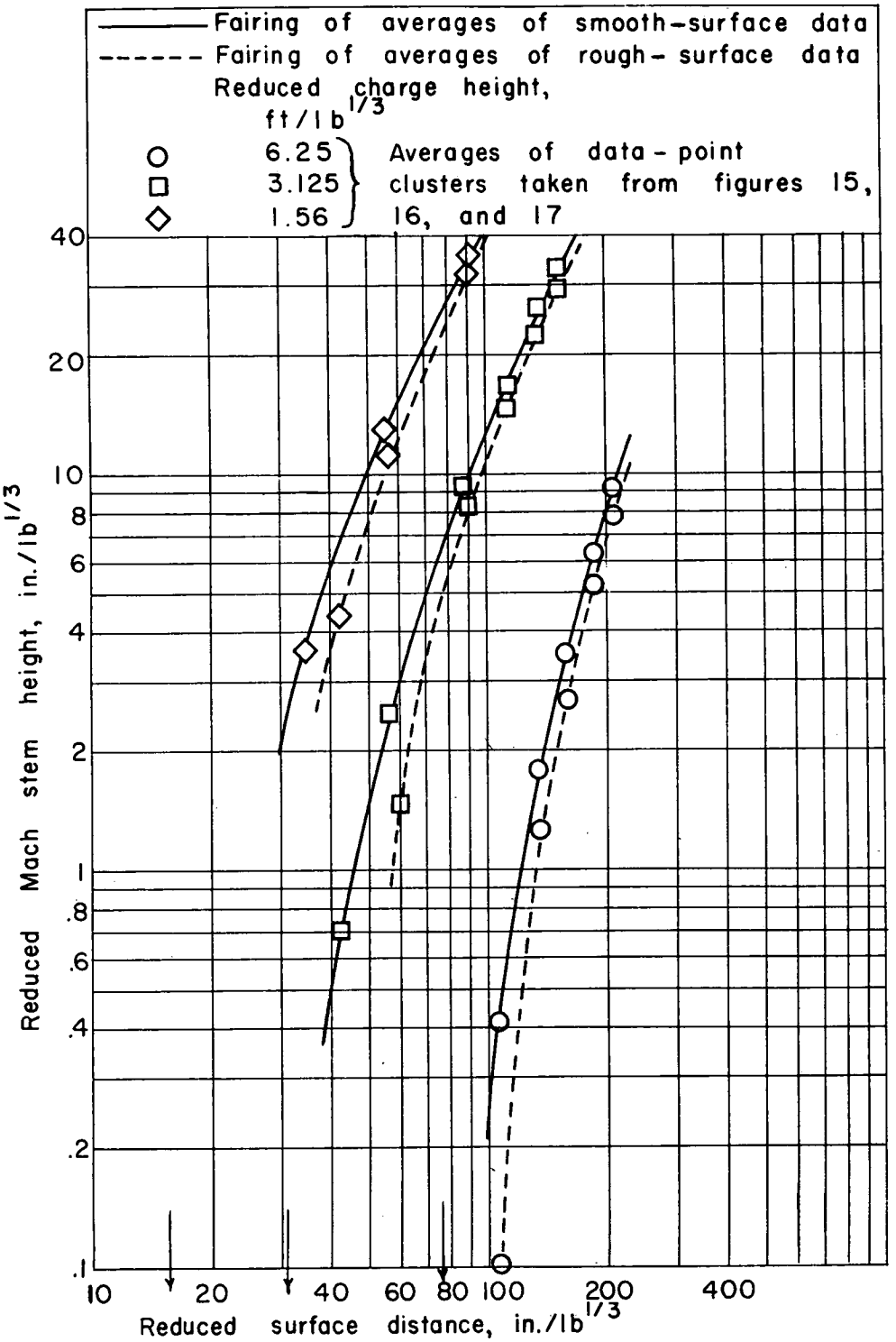

Figure 18.- Comparison of Mach stem growth over smooth and rough surfaces at three heights of burst. Arrows represent abscissas for theoretical points of Mach stem formation.

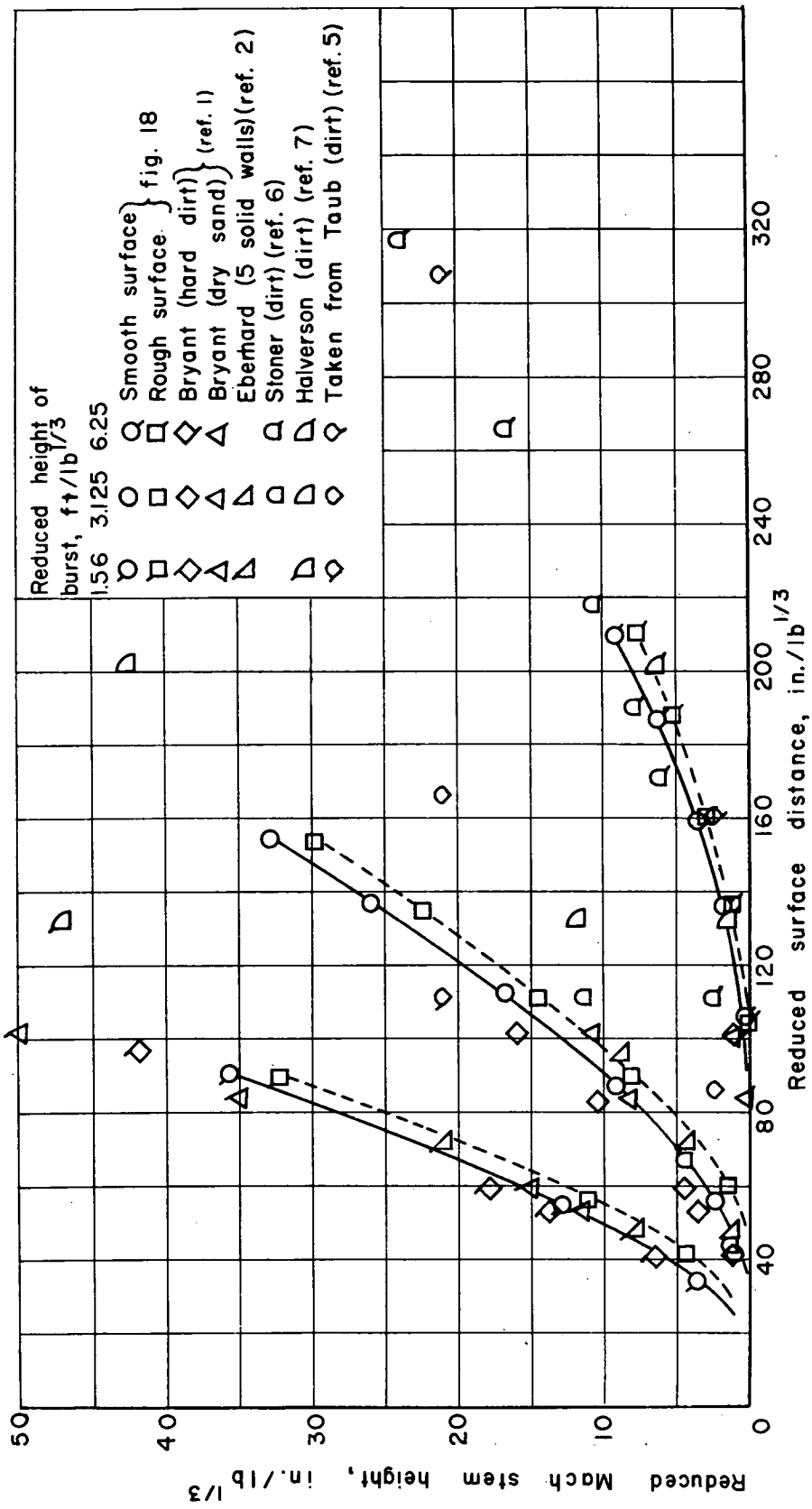

Figure 19.- Comparison of Mach stem growth with reference data.

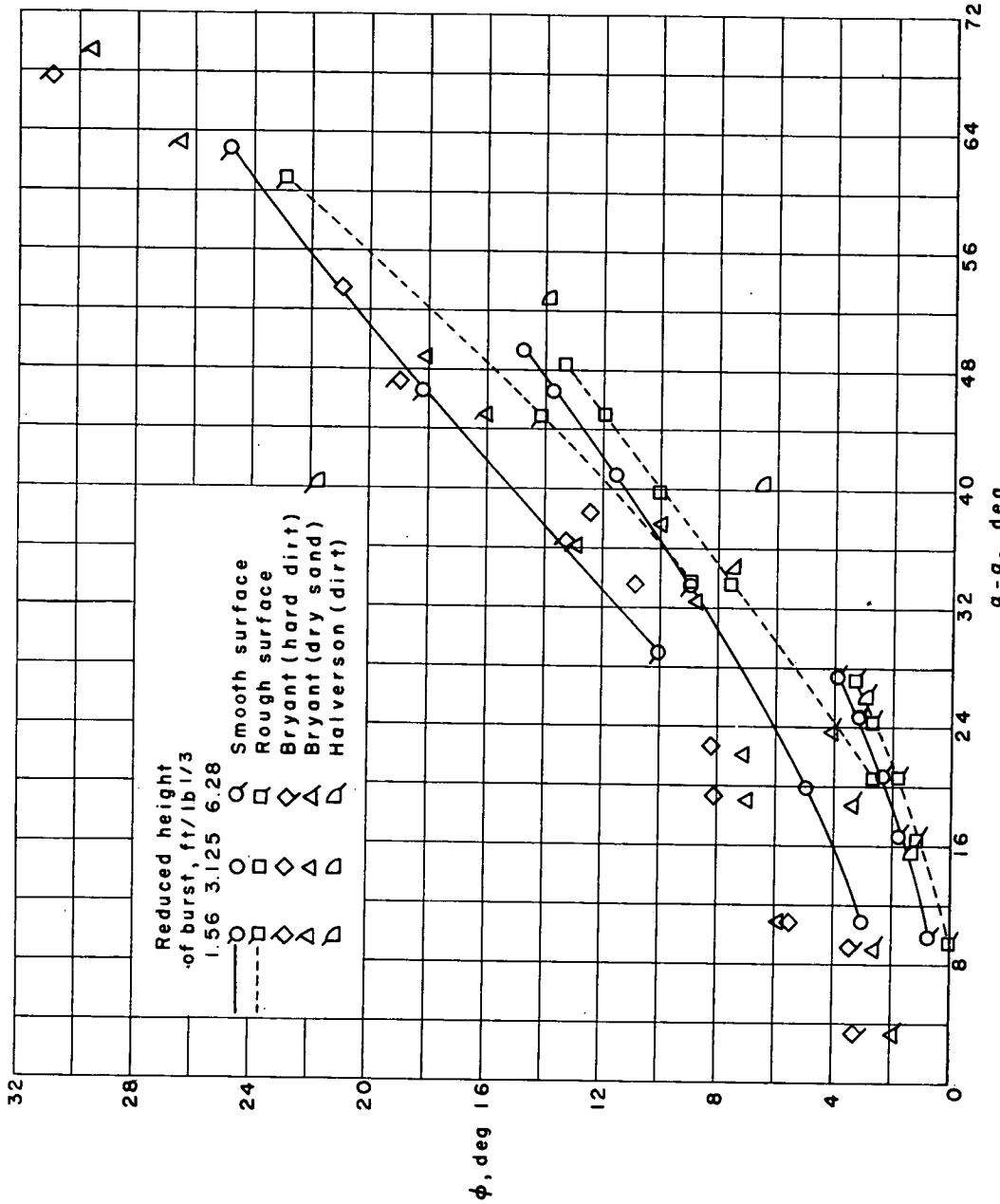

Figure 20.- Path of triple point based on Halverson's height-of-burst similarity parameter.

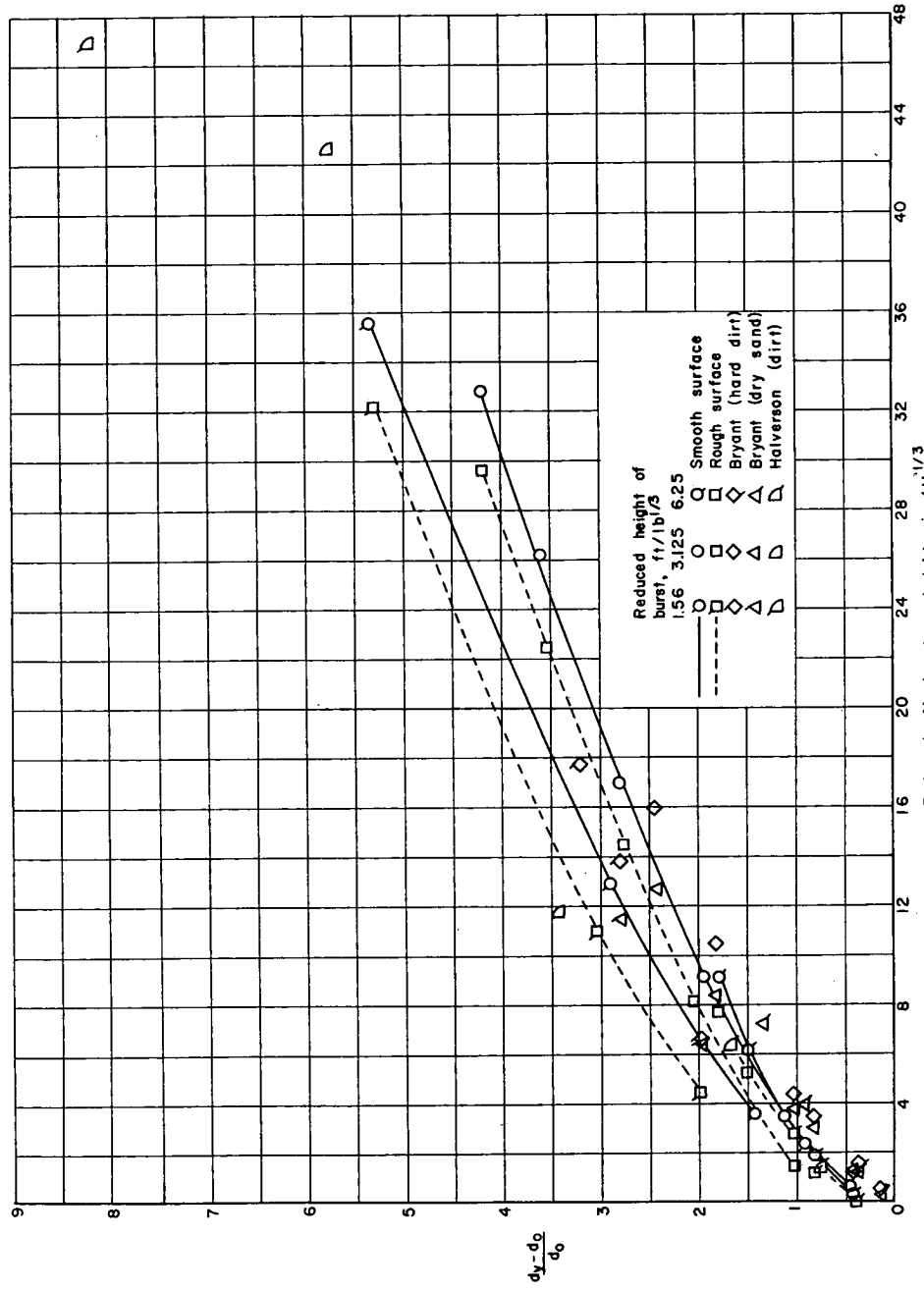

Figure 21.- Approximate similarity of path of triple point rise with height of burst based on $\frac{d_y - d_o}{d_o}$.

NACA-Langley - 5-25-55 - 325